Title: SEDIMENTARY FACIES AND STRATIGRAPHIC ARCHITECTURE OF DEEP-WATER MUDSTONES BEYOND THE BASIN-FLOOR FAN SANDSTONE PINCHOUT

Authors: KÉVIN BOULESTEIX[1*], MIQUEL POYATOS-MORÉ[2], STEPHEN S. FLINT[1], DAVID M. HODGSON[3], KEVIN G. TAYLOR[1], GARETH R. PARRY[3]

Institutions:

[1]School of Earth and Environmental Sciences, University of Manchester, Manchester M13 9PL, UK

[2]Department of Geosciences, University of Oslo, Oslo 0371, Norway

[3]School of Earth and Environment, University of Leeds, Leeds LS2 9JT, UK

Email: kevin.boulesteix@gmail.com

ABSTRACT

Mud dominates volumetrically the fraction of sediment delivered to, and deposited in, deep-water environments, and mudstone is a major component of basin-floor fan systems. However, studies of deep-water successions have mainly focused on their sandstone-prone part, with a consequent bias against the understanding of transport and depositional processes in distal basin-floor positions, and uncertainties about the three-dimensional geometries of deep-water lobes. This study documents the sedimentology and stratigraphy of a distal mudstone-prone basin-floor succession, using a subsurface dataset from the Permian Skoorsteenberg Formation of the Tanqua depocenter (Karoo Basin, South Africa). Macroscopic and microscopic descriptions of five cores from research boreholes (cumulative thickness of 544 m) allowed ten sedimentary facies to be identified, which form five facies associations linked to distinct depositional sub-environments (axis, off-axis, fringe, lobe distal fringe, basin plain). Packages of very thin-bedded mudstones, deposited by waning, low-density turbidity currents stack to form bedsets and bedset packages. Correlation using core suggests they represent the distal fringe of lobes or lobe complexes, and are characterized by various stacking pattern styles (thickening-upward, thinning-upward, thickening-to-thinning upward, constant, variable). Recognition that basin-floor fans pass into distal mudstone beyond the sandstone pinchouts highlights the challenge in adequately identifying the onset of basin-floor fan deposition. Bedsets and bedset packages of lobe distal fringe deposits are separated vertically by basin plain mudstone deposits, characterized by greater bioturbation intensity and total organic carbon, and deposited by lower energy processes (bedload transport by bottom currents, hemipelagic suspension fallout), at time of fan abandonment and sand starvation to the basin-floor. The number of event beds recorded in lobe distal fringe deposits is much higher compared to proximal sandstone-prone basin-floor fan deposits, which illustrates the greater preservation potential of depositional events in distal basin-floor positions. This study highlights the need for more systematic descriptions of deep-water mudstones within basin-floor successions, and the importance of lobe distal fringe deposits for accurate characterization of basin-floor fan architectures, and their use as archives of paleoenvironmental change.

3

INTRODUCTION

Sediments are transported in basin-floor environments by a wide range of processes (low and high density turbidity currents, transitional flows, debris flows, slumps, slides, bottom currents, hemipelagic suspension fallout) (e.g. Bouma 1962; Heezen and Hollister 1964; Middleton and Hampton 1973; Lowe 1982; Stow and Tabrez 1998; Haughton et al. 2003; Kane and Pontén 2012; Talling et al. 2012). These processes contribute to building basin-floor fans (e.g. Mutti 1977; Walker 1978; Nelson et al. 1992; Johnson et al. 2001; Gardner et al. 2003; Hodgson et al. 2006; Deptuck et al. 2008; Prélat et al., 2009; Etienne et al. 2012; Grundvåg et al. 2014). A major component of basin-floor fans are lobes, which can be organized into a five-fold hierarchy (bed, lobe element, lobe, lobe complex, lobe complex set) (Deptuck et al. 2008; Prélat et al. 2009; Grundvåg et al. 2014). Based on vertical and lateral facies associations, lobes can be subdivided into lobe axis, off-axis, fringe and distal fringe (Prélat et al. 2009) (Fig. 1), with a distinction made between frontal and lateral lobe fringes (Spychala et al. 2017). Mudstone/sandstone ratio increases from lobe axis to fringe, and the transition from lobe fringe to distal fringe is marked by the position of the sandstone pinchout (Prélat et al. 2009; Hansen et al. 2019; Fig. 1).

Mud—here defined as <62.5 µm particles (i.e. clay- and silt-size particles; *sensu* Lazar et al. 2015)—dominates volumetrically the fraction of sediments delivered to basin-floor environments. Typically, however, sedimentologic and stratigraphic studies of these deep-water settings have focused on sandstone-prone lobe axis to fringe deposits (e.g. Nelson et al. 1992; Twichell et al. 1992; Satur et al. 2000; Johnson et al. 2001; Hodgson et al. 2006; Etienne et al. 2012; Grundvåg et al. 2014; Spychala et al. 2017; Pierce et al. 2018). As a result, the range of processes transporting and depositing mud in basin-floor environments, beyond the sandstone pinchout, remains relatively understudied. Very thin- to thin-bedded mudstones (*sensu* Campbell 1967) are usually interpreted to be deposited by low-density turbidity currents in lobe distal fringe environments, while homogeneous mudstones are interpreted to be deposited by hemipelagic suspension fallout in the basin plain beyond the lobe reaches (e.g. Johnson et al. 2001; Hodgson et al. 2006; Grundvåg et al. 2014; Spychala et al. 2017). These interpretations are essentially based on macroscopic descriptions from cores and/or outcrops.

However, recent studies using a combination of macroscopic and microscopic description techniques have started to highlight that apparently "homogeneous" deep-water mudstones at core and outcrop scale may be rather characterized by scours, graded beds, and outsized particles (e.g. Schieber 1999; Trabucho-Alexandre et al. 2012; Könitzer et al. 2014; Boulesteix et al. 2019). This suggests that a wider range of processes may be responsible for the transport and deposition of mud in basin-floor environments.

Average dimensions of the sandstone-prone part of lobe (axis to fringe) from Fan 3 of the Skoorsteenberg Formation (Tanqua depocenter, Karoo Basin) are 27 km (length) × 13 km (width) × 5 m (thickness) (Prélat et al. 2009; Fig. 1). However, the dimensions of the mudstone-prone lobe distal fringe deposits have not been established. Therefore, the total dimension of lobes, including the genetically-linked mudstone-prone lobe distal fringe deposits, is unknown. Differentiating mudstones transported and deposited by processes related to lobe distal fringe environments to those basin plain mudstones not genetically linked to any lobes has implications for the correct estimation of deep-water system size (Fig. 1), and for the correct interpretation of depositional rates and sediment mass balance in deep-water environments. This may also aid the stratigraphic prediction of deep-water sandstone hydrocarbon reservoirs in relative up-dip or lateral positions. Lobe distal fringe deposits can also form source rocks (Huc et al. 2001), and host unconventional hydrocarbon accumulations, or act as effective seals. Moreover, anthropogenic pollutants can reach basin-floor environments through transport and deposition by sediment density flows (Kane and Clare 2019; Pierdomenico et al. 2019). Therefore, sedimentologic and stratigraphic characterization of distal basin-floor deposits may also help to predict the extent and volume of pollution in modern basin-floor environments. Distal deep-water successions are also important records for the study of sea-level and paleoclimatic changes (e.g. Schmitz et al. 2001; Zachos et al. 2001; Payros et al. 2012; Bornemann et al. 2014; Dickson et al. 2014; Payros and Martínez-Braceras 2014), since they can offer the continuous record of long time periods, and a potential lower influence of syn- and post-depositional processes (Hillaire-Marcel and Vernal 2007; Ruddiman 2008).

Here, we aim to present for the first time a multi-scale sedimentologic, stratigraphic, and ichnologic study of a mudstone-prone distal basin-floor succession, using an example from the Permian Skoorsteenberg Formation, Karoo Basin, South Africa. Specific objectives of this study are to: 1) characterize the range of transport and depositional processes in mud-prone distal basin-floor environments; 2) describe stacking patterns in distal mudstone-prone basin-floor deposits, and compare them with more proximal sandstone-prone basin-floor deposits; 3) constrain the dimensions of lobes including the distal fringe deposits; 4) discuss sedimentologic, stratigraphic, and ichnologic criteria and implications to differentiate mudstones deposited in lobe distal fringe environments from mudstones unrelated to deep-water lobes.

GEOLOGICAL SETTING

The Karoo Basin (South Africa) has been interpreted as a retroarc foreland basin that formed during the Carboniferous and Permian on the southern margin of Gondwana, with subsidence controlled by flexural loading linked to the development of a magmatic arc and associated fold-thrust belt (Cape Fold Belt) (De Wit and Ransome 1992; Veevers et al. 1994; Visser and Praekelt 1996; Catuneanu et al. 1998; López-Gamundi and Rossello 1998; Viglietti et al. 2017). Alternatively, subsidence during deep-water sedimentation was caused by dynamic topography (mantle flow), linked to the subduction of the paleo-Pacific plate beneath Gondwana (Pysklywec and Mitrovica 1999; Tankard et al. 2009). In this model, loading linked to the development of the Cape Fold Belt occurred later, during the Triassic (Tankard et al. 2009, 2012; Blewett and Phillips 2016).

Located in the south-western corner of the Karoo Basin, the Tanqua depocenter is bounded to the south by the Swartberg Branch and to the west by the Cederberg Branch of the Cape Fold Belt (Fig. 2A). The sedimentary fill comprises the Late Carboniferous to Early Jurassic Karoo Supergroup, subdivided into the glaciogenic Dwyka Group, the post-glacial deep-water to shallow-water Ecca Group, and the continental fluvial Beaufort Group (Fig. 2B) (Smith 1990; Johnson et al. 1996; Catuneanu et al. 2005). The lower Ecca Group (Prince Albert, Whitehill, Collingham and Tierberg

formations) consists of an approximately 600 m-thick mudstone-prone distal basin-floor succession, dominated by sediment-density flow deposits, associated with minor slumps and slides (Fig. 2B) (Visser 1992; Viljoen 1994; Herbert and Compton 2007; Chukwuma and Bordy 2016; Boulesteix et al. 2019). The upper Ecca Group consists of 450 m-thick sandstone-prone basin-floor fans of the Skoorsteenberg Formation (Bouma and Wickens 1994; Wickens 1994; Morris et al. 2000; Johnson et al. 2001; Hodgson et al. 2006) and the 300 m-thick upper slope to shelf deposits of the Waterford Formation (Wild et al. 2009; Dixon et al. 2012; Poyatos-Moré et al. 2016; Gomis-Cartesio et al. 2017, 2018).

The Skoorsteenberg Formation consists of four basin-floor fans (Fans 1-4; Bouma and Wickens 1994), and an overlying slope unit (Unit 5; Wickens 1994; Wild et al. 2009). Grain size range is narrow (mud to fine sand). Integration of field mapping and logging, supplemented by the description and interpretation of 2140 m of continuous core from eleven research boreholes has constrained the sedimentology and stratigraphic architecture of Fans 1-4 (Hodgson et al. 2006; Luthi et al. 2006; Prélat et al. 2009; Spychala et al. 2017; Hansen et al. 2019). Paleocurrent indicators are dominantly to the north/northeast, and the fans are interpreted to be point-sourced from the southwest (Fig. 3B) (Johnson et al. 2001; Hodgson et al. 2006). Fans 1-4 are each up to 65 m thick, and are separated vertically by regionally extensive mudstones (Wickens 1994; Johnson et al. 2001; Hodgson et al. 2006). Each fan is characterized by a progradational-aggradational-retrogradational stacking pattern of constituent lobes (Hodgson et al. 2006). In a sequence stratigraphic framework, Fans 1-4 are each interpreted as a lowstand system tract, while the overlying regionally extensive mudstones are each interpreted to contain the combined expression of transgressive and highstand system tracts (Flint et al. 2011).

This study focuses on the mudstone-prone basin-floor succession situated in a distal position relative to the sandstone-prone sections of Fans 1, 2 and 3 (Fig. 3A). Fan 1 is the least well exposed of the four fans, cropping out in the westernmost part of the Tanqua depocenter (Fig. 3B). Fan 1 has a maximum thickness of 20 m in the southwest, and consists of three sandstone-prone packages separated by mudstone-prone units (Hodgson et al. 2006). Approximately 15 m of mudstone separates

Fan 1 from Fan 2 (Hodgson et al. 2006). Fan 2 is also exposed in the western part of the Tanqua depocenter (Fig. 3B), and has a maximum thickness of 40 m in the southwest. It consists of three sandstone-prone packages also separated by mudstone units. Approximately 35 m of mudstone separates Fan 2 and Fan 3 (Hodgson et al. 2006). A sandstone-prone package is present between Fan 2 and Fan 3 (here named "Interfan 2/3"). Fan 1, Fan 2 and Interfan 2/3 gradually thin to the northeast (Johnson et al. 2001; Hodgson et al. 2006; Fig. 3A).

MATERIALS AND METHODS

The dataset comprises five continuous cores from research boreholes drilled in the Tanqua depocenter (OR01, NB2, NB3, NB4, NS2; Fig. 3A, B). The cores were logged graphically through dry and wet observations (cumulative thickness of 544 m) to record macroscopically visible features including lithology, color, sedimentary structures, bed contacts, bed thicknesses, deformation, trace fossils and bioturbation index. Bioturbation index (BI) of Droser and Bottjer (1986) was used on a 0-5 scale to quantify the intensity of bioturbation, where 0 corresponds to non-bioturbated sediment and 5 corresponds to completely bioturbated sediment. The presence of calcium carbonate was assessed by dropping 5% hydrochloric acid onto the core. Enhanced contrast images of the core using Microsoft Office Picture Manager® helped to capture subtle color changes, bed contacts and trace fossils.

Sixty-three samples were collected from the OR01 core, to study facies and features of interest (stratigraphic surfaces, facies contacts) in details. Thirty-three samples were selected for microscopic analysis to represent the range of facies described from the core. Ultra-thin (20-25 µm thick) oriented polished thin sections (24×46mm) were prepared normal to the bedding orientation. Thin sections were scanned using an Epson Perfection V600 photo scanner at 3200 dpi resolution. Microscopic descriptions were performed using an optical Nikon Eclipse LV100NPOL microscope fitted with a Nikon DS-Fi2 camera. Microscopic descriptions allowed characterization of grain size, mineralogy, bioturbation, bed contacts, grading and diagenetic features. High-resolution imaging and compositional analyse were done on 2 samples using a FEI XL30 environmental scanning electron

microscope (ESEM) with a backscattered electron detector attached at 15 kV, and a working distance of *ca* 10 mm.

Based on the combination of macroscopic and microscopic descriptions, mudstones were classified into different facies following the guidelines of Lazar et al. (2015). Mudstones with more than half the grains <10 µm were classified as fine mudstone, and mudstones with more than half the grains >10 µm as coarse mudstone (e.g. McCave et al. 1995; Lazar et al. 2015). A composition modifier (e.g. siliceous, calcareous, argillaceous and carbonaceous) was added depending on the dominant grain type (quartz, carbonate, clay and organic matter respectively). Stratigraphic changes in ichnodiversity, bioturbation intensity and burrow size were used qualitatively to infer paleo-seafloor physicochemical conditions (oxygen level, sedimentation rate).

Total organic carbon (TOC) from 35 samples (from boreholes NB3, NB4 and NS2) was determined using a LECO SC-144DR. Samples were powdered using a mortar and pestle. Empty sample tubes used for analysis were weighted (m_{tube}). 2 g (+/- 10 %) of sediment per sample was added to the tubes. The tubes with sediment were weighted ($m_{initial}$). Samples were then prepared for total organic carbon analysis by adding 10 % HCL to remove any carbonate content. They were rinsed using distilled water and a centrifuge and dried in an oven at 60°C. The tubes with sediment were weighted after drying (m_{final}). 0.3 g of acid-washed sediment per samples was placed into the LECO to obtain the percentage carbon (P_{OC}). Total organic carbon (TOC) in the samples after carbonate removal was calculated using the formula:

$$TOC = P_{OC} \times ((m_{final} - m_{tube}) / (m_{initial} - m_{tube})). \qquad (1)$$

In order to describe the spatio-temporal distribution of facies in the distal part of the Skoorsteenberg Formation, the five cores have been correlated across the Tanqua depocenter. The base of the ~2 m thick mudstone unit below Fan 3 has been used as a datum for correlation due to its well-constrained regional extent (Hodgson et al. 2006).

FACIES, DEPOSITIONAL PROCESSES AND ICHNOLOGY

Ten distinct facies are observed in the succession. Four mudstone facies (Facies 1-4) are described in detail and interpreted below (Fig. 4). Other illustrations of the four mudstone facies are shown in Figures 5 to 9. Six sandstone facies (Facies 5-10) are summarized in Table 1, from current observations integrated with previous works (e.g. Morris et al. 2000; Johnson et al. 2001; van der Werff and Johnson 2003; Hodgson et al. 2006; Hodgson 2009; Prélat et al. 2009; Jobe et al. 2012; Hofstra et al. 2015; Spychala et al. 2017; Kane et al. 2017). The range of ichnotaxa identified in the succession is shown in Figure 10. TOC values per facies are presented in Figure 11. Facies stacking patterns in the OR01 core is shown in Figure 12, and a correlation panel between the different cores is shown in Figure 13.

Facies 1: Normally Graded Very-Thin Bedded Mudstone

Description.--- Facies 1 consists of light- to mid-gray, argillaceous-siliceous, fine- to coarse-grained bedded mudstone (Fig. 4A, B). Bed thicknesses range from 0.05 to 2 cm (typically <0.5 cm; very thin-bedded, *sensu* Campbell, 1967). Beds are normally graded, usually marked by a light- to dark-gray color grading at core scale (Figs. 4A, 5A), with sharp or erosional bases (Fig. 4B), and some small-scale flame structures (Fig. 4B). Typically, beds comprise a tripartite microstratigraphy (Fig. 5B, C). The basal subdivision consists of laterally continuous to discontinuous planar laminated fine to coarse mudstone. Laminations (usually <1 mm thick) consist of alternating dark- and light-colored laminae with diffuse boundaries (Fig. 5B, C, D). The dark-colored laminae are poorly sorted and consist of clay and organic fragments with rare associated quartz and feldspar (Fig. 5D). The light-colored laminae are well sorted and dominated by quartz and feldspar with rare associated clay and organic fragments (Fig. 5D). The middle subdivision consists of structureless normally graded fine to coarse mudstone (Fig. 5B, C). The upper subdivision consists of ungraded mottled fine mudstone (Fig. 5B, C). The transition from the middle to upper subdivision is either gradual (Fig. 5B) or sharp (Fig. 5C). Part of this facies is characterized by a gradual upward decrease in bed dip angle (Fig. 5A). Facies 1 is locally characterized by soft-sediment deformation (convolute bedding). Texture consists

of clay, quartz and feldspar, with minor associated plant fragments, zircon, apatite, and spore fragments (Fig. 5E). TOC ranges from 0.08 to 0.13 wt.%, with an average of 0.11 wt.% (n = 3) (Fig. 11). Bioturbation is weak to sparse (BI: 1-2), and usually lower in thicker beds (Fig. 4B). Ichnotaxa consist of *Chondrites*, *Helminthopsis*, *Planolites* and *Phycosiphon*, which are generally <0.5-cm in diameter (Fig. 10). The bases of the thickest beds are usually characterized by calcium carbonate cement (Fig. 5B). Macroscopic and microscopic pyrite nodules are rare.

Interpretation.--- Based on the sharp or erosional base, normal grading, and bioturbated top, Facies 1 is interpreted as low-density turbidity current deposits (*sensu* Lowe 1982). The lower planar-laminated bed subdivision indicates deposition from turbulent traction transport (Stow and Piper 1984). The alternation of clay-rich laminae and clay-poor laminae may be explained by cyclic sorting of fine mud and coarse mud by floc breakup in the turbulent boundary layer (Stow and Bowen 1978, 1980). The middle structureless and normally graded subdivision indicates suspension fallout from a waning flow. The upper mottled subdivision indicates suspension fallout from the most dilute part of the flow. The sharp contact between the middle and upper bed subdivisions suggests sediment bypass (e.g. Poyatos-Moré et al. 2016; Boulesteix et al. 2019). Beds with no bypass surface may represent the distal equivalent of beds with a bypass surface (e.g. Boulesteix et al. 2019). Where the lower planar-laminated subdivision is absent, this suggests either: i) primary deposition by traction transport, followed by bioturbation of the laminae (cryptobioturbation *sensu* Pemberton et al. 2008), or ii) deposition by suspension fallout from a waning dilute turbidity current following erosion of the seafloor, without deposition by traction processes. The gradual upward decrease of dip bed angle suggests scour fill at a scale larger than the core width.

Facies 2: Discontinuous Very Thin-Bedded Mudstone

Description.--- Facies 2 consists of light- to mid-gray, argillaceous-siliceous, fine- to coarse-grained mudstone beds (0.05 to 1.5 cm thick, but usually <1 cm thick; very thin-bedded, *sensu* Campbell 1967) (Fig. 4C, D). Beds are usually hard to recognize at core scale, and are laterally discontinuous at the core width (Figs. 4C, 6A). At microscopic scale, bed bases are usually hard to recognize due to

11

biogenic mixing with the underlying bed tops (Fig. 6B). When preserved, bed bases are sharp or erosional (Fig. 6C, D). Similarly to Facies 1, beds are normally graded (Figs. 4D, 6C), while some appear ungraded (Fig. 4D). Texture is similar to Facies 1, with higher clay content (Fig. 6E). TOC values range from 0.14 to 0.24 wt.%, with an average of 0.18 wt.% (*n* = 5) (Fig. 11). Bioturbation is moderate to strong (BI: 3–4), and ichnotaxa consists of *Chondrites, Helminthopsis*, *Planolites* and *Phycosiphon*, similar to Facies 1 (Fig. 10). Burrows are usually larger than in Facies 1 (<2-cm diameter). Macroscopic and microscopic pyrite nodules are more common than in Facies 1 (Fig. 6D).

Interpretation.--- Based on the preserved sharp or erosional bases and normal grading, Facies 2 is interpreted as waning, dilute, low-density turbidity current deposits, similar to Facies 1. Ungraded beds with diffuse contacts suggest strong post-depositional bioturbation.

Facies 3: Very Thin- to Medium-Bedded Structureless Mudstone

Description.--- Facies 3 consists of mid- to dark-gray, siliceous-argillaceous, fine-grained mudstone beds (0.5 to 20 cm thick; very thin- to medium-bedded, *sensu* Campbell 1967) (Fig. 4E, F). Beds are usually weakly normally graded, marked by a light- to dark-gray color grading at core scale (Fig. 7A, B). Bed bases are usually hard to recognize at core scale due to bioturbation, but when recognized they are sharp (Fig. 7A, B), or rarely erosional (Fig. 7C). Beds are structureless, and usually characterized by a white spotty texture at core scale, attributed to *Chondrites* and *Nereites* burrows (Fig. 7A, B). Some beds are bipartite. The lower division consists of a relatively thin (usually <1 cm thick), light-gray structureless and ungraded fine mudstone (Fig. 7A). The upper division is thicker (1-20 cm thick), and consists of a weakly normally graded, light- to dark-gray structureless and mottled fine mudstone (Fig. 7A). Texture consists mainly of clay with minor associated quartz, feldspar, organic fragments and rare zircon, apatite, and spore fragments (Fig. 7D). Compared to Facies 1 and Facies 2, clay and pyrite content is higher, and the texture is usually more poorly sorted (Fig. 7D). TOC values range from 0.09 to 0.27 wt.%, with an average of 0.23 wt.% (n = 4) (Fig. 11). Bioturbation is strong to complete (BI: 4-5), and continuous throughout beds. Ichnotaxa consist of *Chondrites*, *Helminthopsis*, *Nereites*, *Phycosiphon*, *Planolites*, *Teichichnus*, and *Thalassinoides* (Fig.

10). Burrow size is variable, and ranges in diameter from 0.1 cm up to 6 cm. Some burrows are partially filled by calcite and pyrite (Fig. 7A).

Interpretation.--- Based on the sharp or erosional base, and the weak normal grading, Facies 3 is interpreted as deposited from waning, low-density turbidity currents (e.g. Stow et al. 1990). The pervasive bioturbation may be explained by very slow sedimentation (e.g. Stow and Wetzel 1990) which is supported by common pyrite nodules and calcite-filled burrows. Alternatively, this facies may represent completely bioturbated Facies 1 and/or Facies 2 where original individual very-thin beds can be no longer recognized.

Facies 4: Mottled Mudstone

Description.--- Facies 4 consists of mid- to dark-gray, siliceous-argillaceous, fine-grained mottled mudstone (Fig. 4G, H). F4 is structureless and homogeneous at core scale (Fig. 4G). Intensely bioturbated contacts are recognized at core scale, usually associated with calcium carbonate cementation and pyrite nodules (Fig. 10H, J, K, N). These contacts are usually overlain by dark mudstone with common pyrite nodules. At thin-section scale, Facies 4 is commonly characterized by discontinuous planar- to low-angle lamination (Figs. 4H, 8A). Common scours overlain by normally graded or ungraded mudstone are also recognized (Fig. 8B, C). Texture is similar to Facies 3, with higher pyrite content (Fig. 8F). In the upper part of the succession near Fan 3, Facies 4 is usually characterized by the presence of floating coarse mud-sized to medium sand-sized outsize grains (Figs. 9, 12). Outsize grains occur as distinct layers (Fig. 9A), or are randomly distributed within the matrix (Fig. 9B). These grains mostly consist of sub-rounded to sub-angular quartz, polycrystalline quartz, chert, altered feldspar and metamorphic clasts (Fig. 9). They range in diameter from 20 µm to 350 µm (long-axis). TOC values range from 0.15 to 0.48 wt.%, with an average of 0.22 wt.% (*n* = 23) (Fig. 11). Bioturbation is complete (BI: 5), and ichnotaxa consist of *Chondrites*, *Helminthopsis*, *Nereites*, *Phycosiphon*, *Planolites, Teichichnus,* and *Thalassinoides* (Fig. 10), similar to Facies 3. Burrows sizes range from 0.1 cm up to 3 cm in diameter. Some horizons rich in pyrite nodules are characterized by

very small burrows (<0.2 cm diameter), and very low ichnodiversity (dominance of *Chondrites* and *Phycosiphon*).

Interpretation.--- The absence of macroscopic beds and preserved sedimentary structures, associated with the complete bioturbation and high pyrite nodules content, suggest very low sedimentation rate, and deposition by relatively low-energy processes. Microscopic discontinuous laminations may be explained by deposition under bedload transport of fine mud by bottom currents (Schieber et al. 2007, 2011), followed by bioturbation. Scours and normal grading suggest deposition from waning, dilute, low-density turbidity currents, following erosion at the seafloor. Beds with no lamination or scours may be explained by: 1) deposition from suspension fallout; or 2) deposition by bedload transport or by waning, dilute, low-density turbidity currents, followed by complete bioturbation, disrupting the primary sedimentary fabric. Outsized floating grains are larger than any grains found in the fans, and they are interpreted as dropstones, deposited from the melting of sediment-laden seasonal sea ice (e.g. Macquaker and Keller 2005). The evidence for ice-influence sedimentation processes suggests that part of the fine mud in Facies 4 may also originate from the melting of seasonal sea-ice, with deposition by vertical fallout. Alternatively, outsized floating grains may be transported and deposited *en masse* by debris flows. The intensely bioturbated contacts associated with pyrite nodules and calcium-carbonate cementation suggests relatively long breaks in sedimentation (softground to firmground; Ekdale et al. 1984). The horizons with common pyrite nodules and small *Chondrites* and *Phycosiphon* suggest periods of low oxygenation at the seafloor (dysoxiatoanoxia).

FACIES ASSOCIATIONS AND DEPOSITIONAL ENVIRONMENTS

The ten facies described and interpreted in the previous section combine into five facies associations, which are linked to five distinct depositional sub-environments within the basin-floor environment of the Skoorsteenberg Formation (Fig. 14). Note that boundaries between these different depositional sub-environments are transitional.

Lobe Axis, Off-Axis and Fringe

Descriptions and interpretations of lobe axis, off-axis and fringe facies associations are based upon current observations integrated with previous sedimentological studies of the Skoorsteenberg Formation (e.g. Morris et al. 2000; Johnson et al. 2001; van der Werff and Johnson 2003; Hodgson et al. 2006; Luthi et al. 2006; Hodgson 2009; Prélat et al. 2009; Jobe et al. 2012; Hofstra et al. 2015; Spychala et al. 2017; Kane et al. 2017). Lobe axis deposits are 4-8 m thick, and are dominated by amalgamated thick bedded structureless sandstone (Facies 5), commonly associated with structured sandstone (Facies 6) and debrite (Facies 8) (Figs. 12, 14). Lobe off-axis deposits are 2-4 m thick, and are dominated by structured sandstone (Facies 6), commonly associated with structureless sandstone (Facies 5) (Figs. 12, 14). Lobe fringe deposits are 0.1-3 m thick, and consist of very thin- to thin-bedded sandstone (Facies 9), associated with hybrid bed (Facies 7), debrite (Facies 8), structureless sandstone (Facies 5) and structured sandstone facies (Facies 6) (Figs. 12, 14). Frontal fringe deposits are usually characterized by a high proportion of hybrid beds (Facies 7), while lateral fringe deposits are commonly dominated by very thin- to thin-bedded sandstones (Facies 9) (Spychala et al. 2017). Bioturbation intensity and ichnodiversity increases from lobe axis to fringe deposits, which suggest lower physicochemically stressed conditions for benthic organisms in distal basin-floor environments, linked to lower depositional rates and longer depositional breaks (e.g. Heard and Pickering 2008).

Lobe Distal Fringe

Description.--- Commonly, normally graded very thin-bedded mudstones (Facies 1) are associated with discontinuous very thin-bedded mudstones (Facies 2), and rarely with very thin- to thin-bedded sandstones (Facies 9) (Figs. 12, 13, 15, 16). These deposits stack to form bedsets that are 0.05-2.80 m thick, and that usually correlate to lobe axis, off-axis, and fringe deposits (Figs. 13, 16). Facies 1 beds are thicker than Facies 2 beds, and are characterized by a lower bioturbation intensity, smaller burrows and lower average TOC (Fig. 11). Moreover, compared to Facies 2, Facies 1 beds are characterized by small scale flame structures and convolute bedding. Ichnodiversity in both Facies 1 and Facies 2 is relatively low (*Chondrites*, *Helminthopsis*, *Phycosiphon* and *Planolites*; Fig. 10).

Bedsets of Facies 1 and Facies 2 are rarely associated with ash-rich sandstone (Facies 10) and carbonate rich-concretions (Figs. 11, 13, 15, 16).

Interpretation.--- The stacked very thin-bedded nature of Facies 1 and Facies 2 associated with their stratigraphic correlation with lobe axis, off-axis, and fringe deposits, suggest that they represent lobe distal fringe deposits (Fig. 14). This interpretation is consistent with the descriptions and interpretations of stacked very thin-bedded mudstones, intercalated between sandstone-prone lobe deposits from the overlying Fan 3 and Fan 4 (Spychala et al. 2017), and from Unit A of the Laingsburg Formation in the neighbouring Laingsburg depocenter (Prélat and Hodgson 2013). Based on thicker beds, lower bioturbation intensity, smaller burrows, and common convolute bedding and flame structures, Facies 1 is interpreted to record relatively high depositional energy (high sedimentation rate) in the proximal part of the lobe distal fringe environment (Fig. 14), associated with physicochemically stressed conditions for benthic organisms. Comparatively, Facies 2 is characterized by thinner beds, higher bioturbation intensity, bigger burrows, and higher average TOC, which suggest Facies 2 record lower depositional energy (lower sedimentation rate) in the distal part of the lobe distal fringe environment (Fig. 14), associated with a more favorable seafloor environment for benthic organisms. An increase in bioturbation intensity and ichnodiversity from proximal to distal basin-floor fan deposits have also been previously observed in the Basque Basin, Spain (Cummings and Hodgson 2011), in the Jaca Basin, Spain (Heard et al. 2008), in the Annot Basin, France (Phillips et al. 2011), and in the Campanian basin-floor fans of the Norwegian Sea (Knaust 2009). The absence of significant ash-rich sandstone and carbonate-rich concretions associated with Facies 1 and Facies 2 suggests relatively high depositional energy, and no significant breaks in sedimentation in the lobe distal fringe environment.

Basin Plain

Description.--- Very thin- to medium-bedded structureless mudstones (Facies 3) are commonly associated with mottled mudstones (Facies 4), with rare normally graded very thin-bedded mudstones (Facies 1) and discontinuous very thin-bedded mudstones (Facies 2) (Figs. 12, 13, 15, 16). These

packages are 0.1-10 m thick, and are laterally continuous across the Tanqua depocenter (Figs. 13, 16). Compared to lobe distal fringe deposits, packages dominated by Facies 3 and Facies 4 are finer-grained (dominated by fine mudstone), and characterized by a higher bioturbation intensity, larger burrows, and a higher ichnodiversity (*Chondrites*, *Helminthopsis*, *Nereites*, *Phycosiphon*, *Planolites*, *Teichichnus*, *Thalassinoides*; Fig. 10). Moreover, packages dominated by Facies 3 and Facies 4 are more commonly associated with ash-rich sandstones (Facies 10), pyrites nodules, carbonate-rich concretions, and outsize grains (Figs. 12, 15, 16). TOC values are also higher than in lobe distal fringe deposits (Fig. 11).

Interpretation.--- The lateral continuity of packages dominated by Facies 3 and Facies 4, together with common ash-rich sandstones, carbonate-rich concretions, and pyrite nodules, suggest deposition in a low energy basin-plain environment (Fig. 14). High bioturbation intensity, ichnodiversity, and large burrows suggest relatively low depositional energy (low sedimentation rate), associated with favorable oxic seafloor conditions for benthic organisms (Wetzel and Uchman 2012). The presence of outsize grains interpreted as dropstones supports deposition in a low-energy environment (Bennett et al. 1996). Based on the process interpretation of Facies 3 and Facies 4, the basin-plain deposits were accumulated from bottom currents, very dilute low-density turbidity currents, and hemipelagic suspension fallout beyond the reach of flows supplying lobes, or at times when lobes were not active.

STACKING PATTERN

Hierarchy

Distal basin-floor deposits of the Skoorsteenberg Formation are dominated by mudstone facies (Figs. 12, 13, 16). Therefore, the mapping of bounding surfaces between sandstone-prone and mudstone-prone packages, commonly used in more proximal basin-floor fan environments to subdivide stratigraphically the succession (e.g. Prélat et al. 2009; Prélat and Hodgson 2013; Grundvåg et al. 2014) cannot be used in distal basinal environments. Nonetheless, the mudstone-prone distal basin-

floor fan succession is still characterized by a hierarchical vertical and lateral facies arrangement (Figs. 12, 15, 16). We used a similar approach to Prélat et al. (2009) to stratigraphically subdivide the succession, where the lowest energy deposits dominated by Facies 3 and Facies 4 (basin plain facies association) are used as bounding elements to define packages dominated by Facies 1 and Facies 2 (lobe distal fringe facies association) (Fig. 17).

The smallest building blocks in the mudstone-prone distal basin-floor fan environments of the Skoorsteenberg Formation are the very thin beds of Facies 1 and Facies 2 (0.05-2 cm thick with a mean thickness of ~0.2 cm), which represent the deposits of single, waning, low-density turbidity currents. One or more genetically related very thin-beds of Facies 1 and Facies 2 vertically stack to form bedsets (0.005-2.80 m thick, with a mean thickness of 0.08 m), with variable stacking patterns (Figs. 15, 17). Bedsets are sharp based and topped, and are separated vertically by relatively thin (0.05-1 m thick) units dominated by Facies 3 and Facies 4 (basin plain facies association) (Figs. 12, 15, 16, 17). The thin basin plain units separating bedsets can be associated with ash-rich sandstone (Facies 10), carbonate-rich concretions and pyrite nodules (Figs. 12, 15, 16, 17). Some bedsets thin upward, associated with a vertical transition from Facies 1 to Facies 2, and an upward increase in bioturbation intensity (see example from 231.50 m to 230.70 m in OR01; Figs. 12, 17). Other bedsets thicken upward, associated with a vertical transition from Facies 2 to Facies 1, and decreasing-upward bioturbation intensity (see example from 216.75 m to 214.70 m in OR01; Figs. 12, 17). Some bedsets show thickening- then thinning-upward trends, associated with a vertical transition from Facies 2 to Facies 1 to Facies 2, and decreasing- then increasing-upward bioturbation intensity (see example from 287.35 m to 287.05 m in OR01; Figs. 12, 17). Other bedsets are characterized by a less organised stacking patterns, with an alternation of Facies 1 and Facies 2 (see example from 265.9 m up to 264.35 m in OR01; Figs. 12, 17). Finally, some bedsets are characterized by a constant bed thickness, associated with constant bioturbation intensity (see examples from 251.80 m to 251.50 m in OR01; Figs. 12, 17).

Bedsets of Facies 1 and Facies 2 stack vertically to form bedset packages (0.05-5.50 m thick, with a mean thickness of 1.50 m) (Figs. 12, 15, 16, 17). Bedset packages consist of 1 to 16 bedsets, in which

bed stacking pattern is variable (Figs. 15, 17). Some packages thin upward, associated with a vertical transition from bedsets dominated by Facies 1 to bedsets dominated by Facies 2, associated with an increasing-upward bioturbation intensity (see example from 260.70 m to 255.70 m in OR01; Figs. 12, 16). Other bedset packages thicken upwards, associated with a vertical transition from bedsets dominated by Facies 2 to bedsets dominated by Facies 1, and a decreasing-upward bioturbation intensity (see example from 216.70 m to 214.80 m in OR01; Figs. 12, 16). Other packages are thickening- then thinning-upwards associated with a vertical transition from bedsets dominated by Facies 2, to bedsets dominated by Facies 1, and to bedsets dominated by Facies 2, associated with a decreasing- then increasing-upward bioturbation intensity (see example from 253.10 m to 250.30 m in OR01; Fig. 12). Bedset packages are sharp based and sharp topped, and are separated vertically by relatively thick (1.40-6.80 m thick) units dominated by Facies 3 and Facies 4 (basin plain facies association) (Figs. 12, 15, 16). Compared to the thin basin plain units separating bedsets, thicker basin plain units separating bedset packages are more commonly associated with ash-rich sandstone (Facies 10), carbonate-rich concretions, and pyrite nodules (Figs. 12, 15, 16, 17), which suggests lower depositional energy and longer periods of starvation of clastic sediment supply at the basin floor.

Stratigraphic Architecture

Facies interpretation and stratigraphic correlation of cores constrained the stratigraphic architecture of the distal part of the Skoorsteenberg Formation underlying Fan 3 (Figs. 13, 16). The lower part of the succession underlying Fan 2 consists of a section dominated by basin plain mudstone deposits, overlain by four thickening- and coarsening-upwards mudstone-prone bedset packages of lobe distal fringe deposits, which correlate across the study area (Fig. 13). Each bedset package thins and fines away from NB3, and is interpreted as distal fringe deposits of lobes present elsewhere in the Tanqua depocenter. These mudstone-prone packages are overlain by Fan 2, which comprises two sandstone-prone packages (lobe axis to fringe deposits), associated with mudstone-prone lobe distal fringe deposits (Fig. 13). The sandstone-prone lobe axis to fringe deposits of Fan 2 in core NB3 grade to mudstone-prone lobe distal fringe deposits in the other cores. Fan 2 is overlain by two fining- and thinning-upwards bedset packages of mudstone-prone lobe distal fringe deposits that correlate across

the study area with constant thickness (Fig. 13), also interpreted as distal fringe deposits of lobes present elsewhere in the Tanqua depocenter. Interfan 2/3 consists of one bedset package dominated by sandstone-prone lobe axis to fringe deposits in NB3, which thins and grades to mudstone-prone lobe distal fringe in the other cores (Fig. 13).

A 10 m-thick laterally continuous unit dominated by basin plain mudstone deposits overlies Interfan 2/3, with common ash-rich sandstone (Facies 10), overlain by six mudstone-prone bedset packages of lobe distal fringe deposits (Figs. 13, 16). Bedset packages are thicker in NB3, where some are characterized by sandstone-prone fringe deposits (Figs. 13, 16). Each bedset package thins and fines away from NB3, associated with a transition from predominantly Facies 1 to predominantly Facies 2 (Fig. 16). This facies transition is associated with increased bioturbation intensity and greater occurrence and preservation of ash-rich sandstones (Facies 10) and carbonate-rich concretions, which supports lower depositional energy and longer depositional breaks in distal basin-floor environments. These mudstone-prone bedset packages are interpreted as the distal fringes of lobes present elsewhere in the Tanqua depocentre. Bedset packages 1 to 5 pinch-out between NB2 and NS2 cores in distal basin-floor position, while bedset package 6 is laterally continuous across the study area (Fig. 16).

DISCUSSION

Depositional Processes in Distal Basin-Floor Environments

Two mud-prone depositional environments have been described beyond and intercalated with frontal and lateral lobe fringe environments in the distal part of the Skoorsteenberg Formation (lobe distal fringe, basin plain), with distinct facies and dominant transport and depositional processes (Fig. 14). Lobe distal fringe deposits are dominated by very thin-bedded mudstone (Facies 1 and 2), interpreted to be deposited by waning, dilute, low-density turbidity currents at the distalmost end of a lobe. Very thin-bedded mudstones have been previously observed in other distal basin-floor successions (e.g. Wood and Smith 1959; Mutti 1977; Pickering 1981; Bourget et al. 2010; Migeon et al. 2010; Etienne

et al. 2012; Kane and Pontén 2012; Grundvåg et al. 2014). These deposits may represent the distal expression of sediment density flows depositing sandstone in more proximal lobe sub-environments (Fig. 14). Alternatively, they may represent the expression of mud-rich low-density turbidity currents originating from the coeval shelf or slope (e.g. Poyatos-Moré et al. 2016; Boulesteix et al. 2019). In contrast to the very thin beds described in the underlying mudstone-prone Tierberg Formation (Boulesteix et al. 2019), no evidence for hyperpycnal processes (inversely-to-normally graded bed motif) are observed in the Skoorsteenberg Formation mudstones. This may be explained by a more distal position relative to the deltaic sediment delivery system, as a waxing-waning flow is expecting to wane basinward (Kneller and McCaffrey 2003). Alternatively, this may indicate a significant basin margin re-organization, with a transition from a line-sourced to a point-sourced configuration, and sediments transferred to the basin-floor via slope channels (Johnson et al. 2001; Hodgson et al. 2006). Some of the very thin beds of Facies 1 and Facies 2 are characterized by scoured bases (Fig. 5B), which suggest that currents in distal basin-floor positions still had erosive power. The flame structures commonly observed at the base of the thickest beds (Fig. 4B) suggest relatively high sedimentation rates. Some beds are also characterized by sediment bypass surfaces (Fig. 5C). These observations indicate that lobe distal fringe environments, commonly associated with relatively low depositional rates and net sediment accumulation (e.g. Hodgson et al. 2006, Grundvåg et al. 2014), can still record relatively energetic flows and high sedimentation rates, with evidence for sediment bypass to even more distal basin-floor environments.

Basin plain deposits are dominated by strongly bioturbated bedded to non-bedded mudstones (Facies 3 and 4). Their regional extent mean that these deposits dominate volumetrically the succession (Figs. 12, 16), and were previously interpreted as "condensed" deposits, accumulated mostly from hemipelagic suspension fallout (Johnson et al. 2001; Hodgson et al. 2006). Basin plain mudstones were also commonly interpreted as hemipelagic sediments in other deep-water successions (e.g. Grundvåg et al. 2014; Pierce et al. 2018). Here, the basin plain deposits preserve evidence of more energetic processes. Facies 3 beds are characterized by very weak normal grading and pervasive bioturbation, associated with poor-sorting (Fig. 7D), which suggests very slow deposition by

suspension fallout from the dilute cloud of low-density turbidity currents. Similar beds have been described at the distalmost end of the Bengal Fan, where they have been referred as "hemiturbidites", due to their mixed sedimentary characteristics between turbidites and hemipelagites (Stow et al. 1990; Stow and Wetzel 1990). Hemiturbidites are common deposits in other distal basin-floor deposits (e.g. Howe 1996; Plink-Björklund and Steel 2004). The generation of a very dilute plume at the distalmost end of turbidity currents may be explained by buoyancy reversal and lofting after the turbidity current has deposited most of its sediment load in more proximal basin-floor environments (Sparks et al. 1993; Gladstone and Pritchard 2010; Stevenson and Peakall 2010). Facies 4 is macroscopically homogeneous, and can be easily interpreted as hemipelagites without the use of more advanced microscopic analysis. However, microscopic descriptions reveal scours and discontinuous planar- to low-angle laminae (Fig. 8), which suggest other additional depositional processes. Some scours are overlain by normally graded mudstones (Fig. 8B, C), interpreted to be deposited by waning, dilute, low-density turbidity currents following erosion of the seafloor. Laminations in deep-water mudstones are commonly associated with hemipelagic sedimentation and anoxic bottom-water conditions (e.g. Potter et al. 1980; Brodie and Kemp 1994). However, flume experiments have shown that laminations in mudstones can be produced by bedload transport of mud as floccules (Schieber et al. 2007; Schieber and Southard 2007; Schieber and Yawar 2009). Bedload transport may generate low-angle ripples that have a planar laminated appearance after compaction in a wide range of oxic to anoxic bottom-water environments (e.g. Schieber and Yawar 2009; Plint et al. 2012; Trabucho-Alexandre et al. 2012; Plint 2014; Schieber 2016). The common laminations in Facies 4, similar to those generated in flume experiments, suggests that a large proportion of the basin-plain mudstone deposits from the Skoorsteenberg Formation may have accumulated from bedload transport by bottom currents, before being reworked by bioturbation. This suggests that relatively high energy processes were still active on the basin plain when sand was trapped on the shelf or the slope segments of the basin margin. This has implications for the correct estimation of depositional (and compaction) rates in deep-water mudstones (e.g. Kemp et al. 2018), as these basin plain deposits may accumulate episodically. Therefore, hemipelagic sedimentation rates cannot be used for deep-water mudstones, due to the variety of processes remobilizing, transporting and depositing mud on the basin plain.

Distalmost Expression of Lobes

Previous studies of basin-floor fans focused on their sandstone-prone part (lobe axis, off-axis, fringe; e.g. Prélat et al. 2009), with less understanding of the three-dimensional geometry and extension of deep-water lobes beyond sandstone pinchout. Here, we show that the distal mudstone-prone part of the Skoorsteenberg Formation basin-floor fans is characterized by tabular bedsets and bedset packages of very thin-bedded mudstones (Facies 1 and 2), separated by strongly bioturbated bedded-to non-bedded mudstone basin-plain units (Facies 3 and 4) (Figs. 12, 13, 16). Two interpretations have been proposed to explain the presence of very thin-bedded mudstone packages in basin-floor fan successions. In the first, the very thin-bedded mudstone packages are interpreted to indicate an allogenically-driven decrease in sand supply to basin-floor environments during relative sea-level rise, with sand particles trapped on the coeval shelf or slope (e.g. Satur et al. 2000; Johnson et al. 2001; Van der Werff and Johnson 2003; Hodgson et al. 2006; Mulder and Etienne 2010; Flint et al. 2011; Poyatos-Moré et al. 2019). The implication of this interpretation is that the very thin-bedded mudstone packages are not genetically related to sandstone-prone lobes. In the second, very thin-bedded mudstone packages are interpreted as the genetically linked mudstone-prone lobe distal fringe deposits of sandstone-prone lobes present laterally or updip across basin margin, due to autogenic compensational stacking (e.g. Prélat and Hodgson 2013; Spychala et al. 2017). In this study, the stratigraphic correlation of bedset and bedset packages of very thin-bedded mudstones with the sandstone-prone part of basin-floor fans (Figs. 13, 16) support an autogenic origin for these very-thin bedded packages, interpreted to be deposited at the distalmost end of basin-floor fans.

The bedset packages of very-thin bedded mudstones (Facies 1 and 2) immediately below Fan 3 correlate to sandstone-prone lobe fringe deposits in core NB3 (Figs. 13, 16), but no lobe axis and off-axis sandstones have been described at these stratigraphic positions elsewhere in the outcrop belt (Johnson et al. 2001; Hodgson et al. 2006; Prélat et al. 2009). A west-facing gentle intrabasinal slope (~0.1°) confines Fan 3 to the east (Hansen et al. 2019), which suggests that the bedset packages are lateral rather than frontal distal fringes to lobes farther to the west, an area now lost due to erosion. This lateral position is supported by the absence of hybrid beds in NB3, typically associated with

23

frontal lobe fringes (Figs. 12, 16) (Spychala et al. 2017). The 2D nature of the dataset mean we cannot constrain whether each bedset package, interpreted as a lobe, thicken to form lobe complexes to the west. Alternatively, the bedset packages may also correspond to stratigraphically isolated (or disconnected) lobes, marking the initial phase of basin floor sedimentation (e.g. Brooks et al. 2018).

The estimated mean dimension of the sandstone-prone part of lobes (axis, off-axis, fringe) from Fan 3 of the Skoorsteenberg Formation is 13 km in width and 27 km in length (Prélat et al. 2009; Fig. 1). Despite the uncertainties about the exact paleogeographic position of the lobe centroids and paleocurrent directions of the bedsets packages underlying Fan 3, a minimum distance at which lobe distal fringes can be traced beyond lobe fringes can be estimated. Paleocurrent indicators from Fan 3 are to the NNE (Hodgson et al. 2006; Prélat et al. 2009; Spychala et al. 2017), and we assume similar paleocurrent directions for the underlying mudstone-prone bedset packages 1 to 6. The lobe fringe deposits of bedset package 6 in NB3 borehole correlate to lobe distal fringe deposits in NS2 borehole, separated by 18.5 km along the approximate paleoflow direction (Fig. 16). This distance is taken to be a minimum length of lobe distal fringe deposits beyond lobe fringe deposits, which suggests that the minimum length of a lobe is 45.5 km, including the genetically-linked lobe distal fringe deposits. Length to width ratio of the sandstone-prone part of Fan 3 is 2.2 (Prélat et al. 2009). By applying similar ratio for the mudstone-prone lobe distal fringes deposits, the estimated minimum width of the lobe distal fringe is 8.4 km, which suggest that the minimum width of a lobe is 21.4 km, including the genetically-linked lobe distal fringe deposits. The documentation of length scales from lobe fringe to lobe distal fringes suggests that deep-water lobes may be significantly wider/larger than previously estimated, with implications for predicting the presence or absence of genetically-linked deep-water sandstones based on the extension of basin-floor fan influence. Furthermore, this opens the possibility of identifying potentially large basin-floor fan sandstone accumulations by looking carefully at the nature of deep-water mudstone successions at any given locality along basin margins.

Documented thinning rates for the sandstone-prone part of lobes (axis, off-axis, fringe) in unconfined basin-floor environments range from 0.5 m/km - 20 m/km, and the rate is higher in proximal than distal positions (e.g. Weaver et al. 1992; Deptuck et al. 2008; Stevenson et al. 2014; Spychala et al.

2017; Hansen et al. 2019; Fryer and Jobe 2019). However, no thinning rates have been previously estimated for lobe distal fringe deposits. Thinning rates for the lobe distal fringe deposits of the Skoorsteenberg Formation have been estimated in this study between boreholes NB3 and NB2, using the six bedset packages underlying Fan 3 (Fig. 16). These thinning rates are approximate as only two data points are available for bedset package thicknesses, and the direction of the estimated thinning rate relative to the paleocurrent directions is poorly constrained (distal, lateral or oblique). Thinning rates range from 0.0003 m/km (for bedset package 3; Fig. 16), up to 0.003 m/km (for bedset package 2; Fig. 16), with a mean thinning rate of 0.0012 m/km. Despite uncertainties, these values are three-orders of magnitude lower than thinning rates estimated from the sandstone-prone part of basin-floor fans. These very low estimated thinning rates may be explained by the absence of confinement in distal basin floor environments, and by the very dilute nature of the low-density turbidity currents depositing the lobe distal fringes, that allow draping of larger areas of the basin-floor environment, thus generating the observed tabular bodies.

Preservation Potential in Distal Basin-Floor Environments

Based on facies stacking pattern, and correlation with lobe axis to fringe deposits (Figs. 13, 16), bedset packages of very thin-bedded mudstone (Facies 1 and 2) are interpreted to represent the distal fringes of lobes (Prélat et al. 2009). Lobes from the proximal sand-prone Skoorsteenberg Formation (axis to fringe) are 4-10 m thick, and comprise 3 to 10 beds (*sensu* Campbell 1967) in any one vertical section, with an average bed thickness of 0.5 m (Prélat et al. 2009). In comparison, bedset packages of Facies 1 and Facies 2 (lobe distal fringe deposits) are 0.05-5.50 m thick, and consists of 1 to several 1000's of beds, with an average bed thickness of ~0.2 cm. Therefore, there is a major difference in the number of event beds recorded between the proximal sandstone-prone part of a lobe (lobe axis, off-axis and fringe), and the distal mudstone-prone part of a lobe (lobe distal fringe). This difference may be explained by the increasing preservation potential from proximal to distal basin-floor environments.

Lobe axes are prone to amalgamation due to the recurrent avulsion of feeder channels (e.g. Johnson et al. 2001; Gardner et al. 2003; Hodgson et al. 2006; Prélat et al. 2009). Moreover, sediment bypass processes are common in proximal basin-floor environments (e.g. Stevenson et al. 2015). Therefore, the preservation potential of individual beds in these proximal basin-floor fan deposits is low, but increases in lobe off-axis and fringe environments (e.g. Prélat et al. 2009; Spychala et al. 2017). Very thin-bedded mudstones (Facies 1 and 2) are rarely associated with lobe axis to fringe deposits (Figs. 12, 14), although a mud-rich sediment density flow depositing Facies 1 and 2 beds in lobe distal fringe environments may have also deposited mud in more proximal lobe sub-environments. However, the higher energy conditions associated with these proximal depositional environments means the preservation potential of proximal mud deposits is limited, as a subsequent sediment density flow may pick up soft to semi-consolidated mud from the seafloor (rip-up intraclast) and rework it. This mechanism can explain the origin of mud particles and intraclasts in debrites, and the generation of transitional flows and resulting hybrid beds, commonly found in frontal fringe deposits (e.g. Hodgson 2009; Spychala et al. 2017; Kane et al. 2017).

Lower depositional energy in lobe distal fringe environments is supported by higher bioturbation intensity (e.g. Heard et al. 2008; Cummings and Hodgson 2011), associated with more common carbonate-rich concretions and the preservation of ash-rich sandstones (Facies 10). Small-scale erosion and scouring are still observed in these deposits (Figs. 5, 6), but most beds are preserved, with only truncations of the uppermost part of the beds (Figs. 4B, 5B). Therefore, most low-density turbidity currents reaching the lobe distal fringe environments are expected to be preserved in the rock record in the absence of topography. The greater stratigraphic completeness of lobe distal fringe deposits compared to more proximal basin-floor fan deposits means that these mudstone-prone deposits are ideal archives to help decipher allogenic (climate, relative sea level) and autogenic (compensational stacking) signals preserved in the deep-water sedimentary record (e.g. Schmitz et al. 2001; Zachos et al. 2001; Ruddiman 2008; Payros et al. 2012; Bornemann et al. 2014; Dickson et al. 2014; Payros and Martinez-Braceras 2014).

CONCLUSIONS

This integrated study uses a unique subsurface dataset from the Permian Skoorsteenberg Formation of the Tanqua depocenter, Karoo Basin, South Africa, to examine the sedimentology and stacking patterns of deep-water mudstone deposits relative to their proximal equivalent sandstone-prone basin-floor fans. A combination of macroscopic and microscopic description techniques allowed differentiation of ten sedimentary facies, and five facies associations, linked to distinct depositional sub-environments (lobe axis, off-axis, fringe, distal fringe, basin plain). Lobe distal fringe deposits are hierarchically organized, and consist of bedsets and bedset packages of very thin-bedded mudstones, deposited by waning, low-density turbidity currents. Correlation of physical stratigraphy between five continuous cores from research boreholes allowed a genetic link to be established between mudstone-prone lobe distal fringe facies to proximal sandstone-prone lobe facies. Similarly to lobes in proximal sandstone-prone basin-floor fan deposits, bedsets and bedset packages of lobe distal fringes are characterized by various stacking pattern styles (thickening-upward, thinning-upward, thickening-thinning upward, constant, variable). Basin plain mudstone deposits separate vertically bedsets and bedset packages of lobe distal fringes, and consist of strongly bioturbated and structureless mudstones, deposited during periods of basin-floor sand starvation. Common scours and laminations suggest that mud may be transported as bedload by bottom currents during fan abandonment periods. Lobe distal fringe extend for more than 18 km beyond sandstone pinchouts of lobes, with implications for the stratigraphic prediction of deep-water sandstones in updip or lateral positions. The greater number of event beds recorded within lobe distal fringe deposits suggests these successions are a more complete archive of paleoenvironmental change. This study highlights the need for more systematic and integrated descriptions of deep-water mudstones using a range of macroscopic and microscopic description techniques, in order to adequately characterize basin-floor fan architectures, with implications for paleoclimatic and paleogeographic reconstructions.

ACKNOWLEDGEMENTS

REFERENCES

Allen, J.R.L., 1971, Mixing at turbidity current heads, and its geological implications: Journal of Sedimentary Research, v. 41, p. 97-113.

Allen, J.R.L., 1973, A classification of climbing-ripple cross-lamination: Geological Society of London, Journal, v. 129, p. 537-541.

Allen, J.R.L., 1982, Sedimentary Structures: Their Character and Physical Basis. Amsterdam: Elsevier.

Arnott, R.W.C., and Hand, B.M., 1989, Bedforms, primary structures and grain fabric in the presence of suspended sediment rain: Journal of Sedimentary Research, v. 59(6), p. 1062-1069.

Baas, J.H., Best, J.L., and Peakall, J., 2011, Depositional processes, bedform development and hybrid bed formation in rapidly decelerated cohesive (mud-sand) sediment flows: Sedimentology, v. 58(7), 1953-1987.

Bennett, M.R., Doyle, P., and Mather, A.E., 1996, Dropstones: their origin and significance: Palaeogeography, Palaeoclimatology, Palaeoecology, v. 121(3-4), p. 331-339.

Best, J., and Bridge, J., 1992, The morphology and dynamics of low amplitude bedwaves upon upper stage plane beds and the preservation of planar laminae: Sedimentology, v. 39, p. 737-752.

Blewett, S., and Phillips, D., 2016, An overview of Cape Fold Belt geochronology: implications for sediment provenance and the timing of orogenesis. *in* Linol, B., and De Wit, M.J., eds., Origin and Evolution of the Cape Mountains and Karoo Basin, p. 45-55. Springer, Cham.

Bornemann, A., Norris, R.D., Lyman, J.A., D'haenens, S., Groeneveld, J., Röhl, U., Farley, K.A., and Speijer, R.P., 2014, Persistent environmental change after the Paleocene-Eocene Thermal Maximum in the eastern North Atlantic: Earth and Planetary Science Letters, v. 394, p. 70-81.

Boulesteix, K., Poyatos-Moré, M., Flint, S.S., Taylor, K.G., Hodgson, D.M., and Hasiotis, S.T., 2019, Transport and deposition of mud in deep-water environments: processes and stratigraphic implications: Sedimentology. doi: 10.1111/sed.12614

Bouma, A.H., 1962, Sedimentology of some flysch deposits: A graphic approach to facies interpretation: New York: Elsevier. 168 p.

Bouma, A.H., and Wickens H.D.V., 1994, Tanqua Karoo, ancient analog for fine-grained submarine fans, Submarine fans and turbidite systems. GCSSEPM Foundation 15th Annual Research Conference, v. 23.

Bourget, J., Zaragosi, S, Mulder, T., Schneider, J.L., Garlan, T., Van Toer, A., Mas, V., and Ellouz-Zimmermann, N., 2010, Hyperpycnal-fed turbidite lobe architecture and recent sedimentary processes: A case study from the Al Batha turbidite system, Oman margin: Sedimentary Geology, v. 229, p. 144-159.

Brodie, I., and Kemp, A.E.S., 1994, Variation in biogenic and detrital fluxes and formation of laminae in late Quaternary sediments from the Peruvian coastal upwelling zone: Marine and Petroleum Geology, v. 116(3-4), p. 385-398.

Brooks, H.L., Hodgson, D.M., Brunt, R.L., Peakall, J., Poyatos-Moré, M., and Flint, S.S., 2018, Disconnected submarine lobes as a record of stepped slope evolution over multiple sea-level cycles: Geosphere, v. 14(4), 1753-1779.

Campbell, C.V., 1967, Lamina, laminaset, bed and bedset: Sedimentology, v. 8(1), p. 7-26.

Catuneanu, O., Hancox, P.J., and Rubidge, B.S., 1998, Reciprocal flexural behaviour and contrasting stratigraphies: a new basin development model for the Karoo retroarc foreland system, South Africa: Basin Research, v. 10, p. 417-439.

Catuneanu, O., Wopfner, H., Eriksson, P.G., Cairncross, B., Rubidge, B.S., Smith, R.M.H., and Hancox, P.J., 2005, The Karoo basins of south-central Africa: Journal of African Earth Sciences, v. 43, p. 211-253.

Chukwuma, K., and Bordy, E.M., 2016, Spatiotemporal sedimentary facies variations in the Lower Permian Whitehill Formation, Ecca Group, Karoo Basin. *in* Linol, B., and De Wit, M.J., eds., Origin and Evolution of the Cape Mountains and Karoo Basin, p. 101-110. Springer, Cham.

Cummings, J.P., and Hodgson, D.M., 2011, Assessing controls on the distribution of ichnotaxa in submarine fan environments, the Basque Basin, Northern Spain: Sedimentary Geology, v. 239, p. 162-187.

De Wit, M.J., and Ransome, I.G.D., 1992, Regional inversion tectonics along the southern margin of Gondwana. *in* De Wit, M.J., and Ransome, I.G.D., eds., Inversion tectonics of the Cape Fold Belt, Karoo and Cretaceous Basins of Southern Africa, p. 15-21.

Deptuck, M.E., Piper, D.J.W., Savoye, B., and Gervais, A., 2008, Dimensions and architecture of late Pleistocene submarine lobes off the northern margin of East Corsica: Sedimentology, v. 55, p. 869-898.

Dickson, A.J., Rees-Owen, R.L., März, C., Coe, A.L., Cohen, A.S., Pancost, R.D., Taylor, K., and Shcherbinina, E., 2014, The spread of marine anoxia on the northern Tethys during the Paleocene-Eocene Thermal Maximum: Paleoceanography and Paleoclimatology, v. 29(6), p. 471-488.

Dixon, J.F., Steel, R.J., and Olariu, C., 2012, River-dominated, shelf-edge deltas: delivery of sand across the shelf break in the absence of slope incision: Sedimentology, v. 59, p. 1133-1157.

Droser, M.L., and Bottjer, D.J., 1986, A semiquantitative field classification of ichnofabric: Journal of Sedimentary Research, v. 56(4), p. 558-559.

Ekdale, A.A., Bromley, R.G., and Pemberton, S.G., 1984, Ichnology—Trace Fossils in Sedimentology and Stratigraphy: SEPM Short Course Notes, v. 15

Etienne, S., Mulder, T., Bez, M., Desabliaux, G., Kwasniewski, A., Parize, O., Dujoncquoy, E., and Salles, T., 2012, Multiple scale characterization of sand-rich distal lobe deposit variability: examples from the Annot Sandstones Formation, Eocene-Oligocene, SE France: Sedimentary Geology, v. 273-274, p. 1-18.

Flint, S.S., Hodgson, D.M., Sprague, A.R., Brunt, R.L., Van der Merwe, W.C., Figueiredo, J., Prélat, A., Box, D., Di Celma, C., and Kavanagh, J.P., 2011, Depositional architecture and sequence stratigraphy of the Karoo Basin floor to shelf edge succession, Laingsburg depocenter, South Africa: Marine and Petroleum Geology, v. 28, p. 658-674.

Fryer, R.C., and Jobe, Z.R., 2019, Quantification of the bed-scale architecture of submarine depositional environments: The Depositional Record, v. 5(2).

Gardner, M.H., Borer, J.M., Melick, J.J., Mavilla, N., Dechesne, M., and Wagerle, R.N., 2003, Stratigraphic process-response model for submarine channels and related features from studies of Permian Brushy Canyon outcrops, West Texas: Marine and Petroleum Geology, v. 20, p. 757-787.

Gladstone, C., and Pritchard, D., 2010, Patterns of deposition from experimental turbidity currents with reversing buoyancy: Sedimentology, v. 51(1), p. 53-84.

Gomis-Cartesio, L.E., Poyatos-Moré, M., Flint, S.S., Hodgson, D.M., Brunt, R.L., and Wickens, H.D.V., 2016, Anatomy of a mixed-influence shelf edge delta, Karoo Basin, South Africa: Geological Society London, Special Publication, v. 444, p. 393-418.

Gomis-Cartesio, L.E., Poyatos-Moré, M., Hodgson, D.M., and Flint, S.S., 2018, Shelf-margin clinothem progradation, degradation and readjustement: Tanqua depocenter, Karoo Basin (South Africa): Sedimentology, v. 65, p. 809-841.

Grundvåg, S.A., Johannessen, E.P, Helland-Hansen, W., and Plink-Björklund, P., 2014, Depositional architecture and evolution of progradationally stacked lobe complexes in the Eocene Central Basin of Spitsbergen: Sedimentology, v. 61, p. 535-569.

Hansen, L.A.S., Hodgson, D.M., Pontén, A., Bell, D., and Flint, SS., 2019, Quantification of basin-floor floor fan pinchouts: Example from the Karoo Basin, South Africa: Frontiers in Earth Science, v. 7.

Haughton, P.D.W., Barker, S.P., and McCaffrey, W.D., 2003, Linked debrites in sand-rich turbidite systems-origin and significance: Sedimentology, v. 50(3), p. 459-482.

Haughton, P.D.W., Davis, C., McCaffrey, W.D., and Barker, S.P., 2009, Hybrid sediment gravity flow deposits – Classification, origin and significance: Marine and Petroleum Geology, v. 26, p. 1900-1918.

Heard, T.G., and Pickering, K.T., 2008, Trace fossils as diagnostic indicators of deep-marine environments, Middle Eocene Ainsa-Jaca basin, Spanish Pyrenees: Sedimentology, v. 55, p. 809-844.

Heezen, B.C., and Hollister, C., 1964, Deep-sea current evidence from abyssal sediments: Marine Geology, v. 1(2), p. 141-174.

Herbert, C.T., and Compton, J.S., 2007, Depositional environments of the lower Permian Dwyka diamictite and Prince Albert shale inferred from the geochemistry of early diagenetic concretions, southwest Karoo Basin, South Africa: Sedimentary Geology, v. 194, p. 263-277.

Hillaire-Marcel, C., and De Vernal, eds., Proxies in Late Cenozoic Paleoceanography, v. 1, 2007.

Hodgson, D.M., Flint, S.S., Hodgetts, D., Drinkwater, N.J., Johannessen, E.P., and Luthi, S.M., 2006, Stratigraphic evolution of a fine-grained submarine fan systems, Tanqua Depocenter, Karoo Basin, South Africa: Journal of Sedimentary Research, v. 76, p. 20-40.

Hodgson, D.M., 2009, Distribution and origin of hybrid beds in sand-rich submarine fans of the Tanqua depocentre, Karoo Basin, South Africa: Marine and Petroleum Geology, v. 26(10), p. 1940-1956.

Hofstra, M., Hodgson, D.M., Peakall, J., and Flint, S.S., 2015, Giant scour-fills in ancient channel-lobe transition zones: Formative processes and depositional architecture: Sedimentary Geology, v. 329, p. 98-114.

Howe, J.A., 1996, Turbidite and contourite sediment waves in the northern Rockall Trough, North Atlantic Ocean: Sedimentology, v. 43(2), p. 219-234.

Huc, A.Y., Bertrand, P., Stow, D.A.V., Gayet, J., and Vandenbroucke, M., 2001, Organic sedimentation in deep offshore settings: the Quaternary sediments approach: Marine and Petroleum Geology, v. 18, p. 513-517.

Hunter, R.E., 1977, Terminology of cross-stratified sedimentary layers and climbing-ripple structures: Journal of Sedimentary Research, v. 47, p. 697-706.

Iverson, R.M., Reid, M.E., and Lahusen, R.G., 1997, Debris-flow remobilization from landslides: Annual Review of Earth Planetary Sciences, v. 25(1), p. 85-138.

Jobe, Z.R., Lowe, D.R., and Morris, W.R., 2012, Climbing-ripple successions in turbidite systems: depositional environments, sedimentation rates and accumulation times: Sedimentology, v. 59, p. 867–898.

Johnson, M.R., Van Vuuren, C.J., Hegenberger, W.F., Key, R., and Show, U., 1996, Stratigraphy of the Karoo Supergroup in southern Africa: an overview: Journal of African Earth Sciences, v. 23(1), p. 3-15.

Johnson, S.D., Flint, S.S., Hinds, D., and Wickens, H.D.V., 2001, Anatomy, geometry and sequence stratigraphy of basin floor to slope turbidite systems, Tanqua Karoo, South Africa: Sedimentology, v. 48, p. 987-1023.

Jopling, A.V., and Walker, R.G., 1968, Morphology and origin of ripple-drift cross-lamination, with examples from the Pleistocene of Massachusetts: Journal of Sedimentary petrology, v. 38, p. 971-984.

Kane, I.A., and Pontén, A.S.M., 2012, Submarine transitional flow deposits in the Paleogene Gulf of Mexico: Geology, v. 40, p. 1119-1122.

Kane, I.A., Pontén, A.S.M., Vangdal, B., Eggenhuisen, J.T., Hodgson, D.M., and Spychala, Y.T., 2017, The stratigraphic record and processes of turbidity current transformation across dep-marine lobes: Sedimentology, v. 64(5), p. 1236-1273.

Kane, I.A., and Clare, M.A., 2019, Dispersion, accumulation, and the ultimate fate of microplaticss in deep-marine environments: A review and future directions: Frontiers in Earth Science.

Kemp, D.B., Fraser, W.T., and Izumi, K., 2018, Stratigraphic completeness and resolution in an ancient mudrock succession: Sedimentology, v. 65, p. 1875-1890.

Knaust, D., 2009, Characterisation of a Campanian deep-sea fan system in the Norwegian Sea by means of ichnofabrics: Marine and Petroleum Geology, v. 26, p. 1199-1211.

Kneller, B.C., and Branney, M.J., 1995, Sustained high-density turbidity currents and the deposition of thick massive sands: Sedimentology, v. 42(4), p. 607-616.

Kneller, B.C., and McCaffrey, W.D., 2003, The interpretation of vertical sequences in turbidite beds: The influence of longitudinal flow structure: Journal of Sedimentary Research, v. 73(5), p. 706-713.

Könitzer, S.F., Davies, S.J., Stephenson, M.H., and Leng, M.J., 2014, Depositional controls on mudstone lithofacies in a basinal setting: implications for the delivery of sedimentary organic matter: Journal of Sedimentary Research, v. 84, p. 198-214.

Lazar, R.O., Bohacs, K.M., Macquaker, J.H.S., Schieber, J., and Demko, T.M., 2015, Capturing key attributes of fine-grained sedimentary rocks in outcrops, cores, and thin sections: nomenclature and description guidelines: Journal of Sedimentary Research, v. 85, p. 230-246.

Leclair, S.F., and Arnott, R.W.C., 2005, Parallel lamination formed by high-density turbidity currents: Journal of Sedimentary Research, v. 75(1), p. 1-5.

López-Gamundi, O., and Rossello, E.A., 1998, Basin fill evolution and paleotectonic patterns along the Samfrau geosyncline: the Sauce Grande basin-Ventana foldbelt (South Africa) revisited: Geologische Rundschau, v. 86, p. 819-834.

Lowe, D.R., 1982, Sediment gravity flows: II, Depositional models with special reference to the deposits of high-density turbidity currents: Journal of Sedimentary Research, v. 52, p. 279-297.

Luthi, S.M., Hodgson, D.M., Geel, C.R., Flint, S.S., Goedbloed, J.W., Drinkwater, N.J., and Johannessen, E.P., 2006, Contribution of research borehole data to modelling fine grained turbidite reservoir analogues, Permian Tanqua–Karoo basin-floor fans (South Africa): Petroleum Geosciences, v. 12, p. 175–190.

Macquaker, J.H.S., and Keller, M.A., 2005, Mudstone sedimentation at high latitudes: Ice as a transport medium for mud and supplier of nutrients: Journal of Sedimentary Research, v. 75(4), p. 696-709.

McCave, I.N., Manighetti, B., and Robinson, S.G., 1995, Sortable silt and fine sediment size/composition slicing: Parameters for palaeocurrent speed and palaeoceanography: Paleoceanography, v. 10(3), p. 593-610.

Middleton, G.V., and Hampton, M.A., 1973, Sediment gravity flows: Mechanics of flow and deposition. *in* Middleton, G.V., Bouma, A.H., eds., Turbidites and deep water sedimentation: Pacific Section. Society of Economic Paleontologists and Mineralogists Book 2, Short Course Notes, 1–38.

Migeon, S., Ducassou, E., Le Gonidec, Y., Rouillard, P., Mascle, J., and Revel-Rolland, M., 2010, Lobe construction and sand/mud segregation by turbidity currents and debris flows on the western Nile deep-sea fan (Eastern Mediterranean): Sedimentary Geology, v. 229(3), p. 124-143.

Morris, W.R., Scheilhing, M.H., Wickens, H.D.V., and Bouma, A.H., 2000, Reservoir architecture of deepwater sandstones: examples from the Skoorsteenberg Formation, Tanqua Karoo Sub-Basin, South Africa. *in* Weimer, P., Slatt, R.M., Bouma, A.H., and Lawrence, D.T., eds., Deep-Water Reservoirs of the World: SEPM, Gulf Coast Section, Twentieth Annual Research Conference, p. 1010–1032.

Mulder, T., and Etienne, S., 2010, Lobes in deep-sea turbidite systems: State of the art: Sedimentary Geology, v. 229, p. 75-80.

Mutti, E., 1977, Distinctive thin-bedded turbidites facies and related depositional environments in the Eocene Hecho Group (South-central Pyrenees, Spain): Sedimentology, v. 24, p. 107-131.

Nelson, C.H., Twhichell, D.C., Schwab, W.C., Lee, H.J., and Kenyon, N.H., 1992, Upper Pleistocene turbidite sand beds and chaotic silt beds in the channelized, distal, outer-fan lobes of the Mississippi Fan: Geology, v. 20, p. 693-696.

Payros, A., Ortiz, S., Alegret, L., Orue-Etxebarria, X., Apellaniz, E., and Molina, E., 2012, An early Lutetian carbon-cycle perturbation: Insights from the Gorrondatxe section (western Pyrenees, Bay of Biscay): Paleoceanography and Paleoclimatology, v. 27(2).

Payros, A., and Martínez-Braceras, N., 2014, Orbital forcing in turbidite accumulation during the Eocene greenhouse interval: Sedimentology, v. 61, p. 1411-1432.

Pemberton, S.G., McEachern, J.A., Gingras, M.K., and Saunders, T.D., 2008, Biogenic chaos: Cryptobioturbation and the work of sedimentologically friendly organisms: Palaeogeography, Palaeoclimatology, Palaeoecology, v. 270(3-4), p. 273-279.

Phillips, C., McIlroy, D., and Elliot, T., 2011, Ichnological characterization of Eocene/Oligocene turbidites from the Grès d'Annot Basin, French Alps, SE France: Palaeogeography, Palaeoclimatology, Palaeoecology, v. 300(1-4), p. 67-83.

Pickering K.T., 1981, Two types of outer fan lobe sequence, from the late Precambrian Kongsfjord Formation submarine fan, Finnmark, North Norway: Journal of Sedimentary Research, v. 51(4), p. 1277-1286.

Pierce, C.S., Haughton, P.D.W., Shannon, P.M., Pulham, A.J., Barker, S.P., and Martinsen, O.J., 2018, Variable character and diverse origin of hybrid event beds in a sandy submarine fan system, Pennsylvanian Ross Sandstone Formation, western Ireland: Sedimentology, v. 65, p. 952-992.

Pierdomenico, M., Casalbore, D., and Chiocci, F.L., 2019, Massive benthic litter funnelled to deep sea by flash-flood generated hyperpycnal flows: Scientific Reports, v. 9(1).

Plink-Björklund, P., and Steel, R.J., 2004, Initiation of turbidity currents: outcrop evidence for Eocene hyperpycnal flow turbidite: Sedimentary Geology, v. 165(1-2), p. 29-52.

Plint, A.G., Macquaker, J.H.S., and Varban, B.L., 2012, Bedload transport of mud across a wide, storm-influenced ramp: Cenomanian-Turonian Kaskapau Formation, Western Canada foreland Basin: Journal of Sedimentary Research, v. 82, p. 801-822.

Plint, A.G., 2014, Mud dispersal across a Cretaceous prodelta: Storm-generated, wave-enhanced sediment gravity flows inferred from mudstone microtexture and microfacies: Sedimentology, v. 61, p. 609-647.

Potter, P.E., Maynard, J.B., and Pryor, W.A., 1980, Sedimentology of Shale: New York, Springer-Verlag, 306 p.

Poyatos-Moré, M., Jones, G.D., Brunt, R.L., Hodgson, D.M., Wild, R.J., and Flint, S.S., 2016, Mud-dominated basin-margin progradation: Processes and implications: Journal of Sedimentary Research, v. 86, p. 863-878.

Poyatos-Moré, M., Jones, G.S., Brunt, R.L., Tek, D.E., Hodgson, D.M., and Flint, S.S., 2019, Clinoform architecture and along-strike facies variability through an exhumed erosional to accretionary basin margin transition: Basin Research. DOI: 10.1111/bre.12351

Prélat, A., Hodgson, D.M., and Flint, S.S., 2009, Evolution, architecture and hierarchy of distributary deep-water deposits: a high resolution outcrop investigation from the Permian Karoo Basin, South Africa: Sedimentology, v. 56, p. 2132-2154.

Prélat, A., and Hodgson, D.M., 2013, The full range of turbidite bed thickness patterns in submarine lobes: controls and implications: Journal of the Geological Society, London, v. 170, p. 209-214.

Pysklywec, R.N., and Mitrovica, J.X., 1999, The role of subduction-induced subsidence in the evolution of the Karoo Basin: The Journal of Geology, v. 107(2), p. 155-164.

Ruddiman, W.F., 2001, Earth's Climate: past and future. Macmillan.

Satur, N., Hurst, A., Cronin, B.T., Kelling, G., and Gürbüz, K., 2000, Sand body geometry in a sand-rich, deep-water clastic system, Miocene Cingöz Formation of southern Turkey: Marine and Petroleum Geology, v. 17(2), p. 239-252.

Schieber, J., 1999, Distribution and deposition of mudstone facies in the Upper Devonian Sonyea Group of New York: Journal of Sedimentary Research, v. 69, p. 909-925.

Schieber, J., Southard, J., and Thaisen, K., 2007, Accretion of mudstone beds from migrating floccule ripples: Science, v. 318(5857), p. 1760-1763.

Schieber, J., and Yawar, Z., 2009, A new twist on mud deposition – Mud ripples in Experiment and rock record: The Sedimentary Record, v. 7(2), p. 4-8

Schieber, J., 2011, Reverse engineering mother nature-shale sedimentology from an experimental perspective: Sedimentary Geology, v. 238 (1-2), p. 1-22.

Schieber, J., 2016, Mud-redistribution in epicontinental basins – Exploring likely processes: Marine and Petroleum Geology, v. 71, p. 119-133.

Schmitz, B., Pujalte, V., and Betelu, K., 2001, Climate and sea-level perturbations during the incipient Eocene Thermal Maximum: evidence from siliciclastic units in the Basque Basin (Ermua, Zumaia and
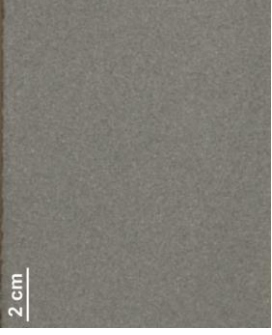
Trabakua Pass), northern Spain: Palaeogeography, Palaeoclimatology, palaeoecology, v. 165, p. 299-320.

Smith, R.M.H., 1990, A review of stratigraphy and sedimentary environments of the Karoo Basin of South Africa: Journal of African earth Sciences, v. 16(1-2), p. 143-169.

Southard, J.B., 1991, Experimental determination of bed-form stability: Annual Review of Earth and Planetary Science, v. 19, p. 423-455.

Sparks, R.S.J., Bonnecaze, R.T., Huppert, H.E., Lister, J.R., Hallworth, M.A., Mader, H., and Phillips, J., 1993, Sediment-laden gravity currents with reversing buoyancy: Earth and Planetary Science Letters, v. 114(2-3), p. 243-257.

Spychala, Y.T., Hodgson, D.M., Prélat, A., Kane, I.A., Flint, S.S., and Mountney, N.P., 2017, Frontal and lateral submarine lobe fringes: Comparing sedimentary facies, architecture and flow processes: Journal of Sedimentary Research, v. 87, p. 75-96.

Stevenson, C.J., and Peakall, J., 2010, Effects of topography on lofting gravity flows: Implications for the deposition of deep-water massive sands: Marine and Petroleum Geology, v. 27(7), p. 1366-1378.

Stevenson, C.J., Talling, P.J., Sumner, E.J., Masson, D.G., Frenz, M., and Wynn, R.B., 2014, On how thin submarine flows transported large volumes of sand for hundreds of kilometres across a flat basin plain without eroding sea floor: Sedimentology, v. 61(7), p. 1982-2019.

Stevenson, C.J., Jackson, C.A.L., Hodgson, D.M., Hubbard, S.M., and Eggenhuisen, J.T., 2015, Deep-water sediment bypass: Journal of Sedimentary Research, v. 85(9), p. 1058-1081.

Stow, D.A.V., and Bowen, A.J., 1978, Origin of lamination in deep sea, fine-grained sediments: Nature, v. 274, p. 324-328.

Stow, D.A.V., and Bowen, A.J., 1980, A physical model for the transport and sorting of fine-grained sediment by turbidity currents: Sedimentology, v. 27(1).

Stow, D.A.V., and Piper, D.J.W., 1984, Deep-water fine-grained sediments: facies models: Geological Society, London, Special Publications, v. 15(1), p. 611-646.

Stow, D.A.V., Amano, K., Balson, P.S., Brass, G.W., Corrigan, J., Raman, C.V., Tiercelin, J.J., Townsend, M., and Wijayananda, N.P., 1990, Sediment facies and processes on the distal Bengal Fan, Leg 116. *in* Cochran, J.R., Stow, D.A.V., et al. eds., Proceedings of the Ocean Drilling Project, Leg, v. 116, p. 377-396.

Stow, D.A.V., and Wetzel, A., 1990, Hemiturbidite: a new type of deep-water sediment. *in* Proceedings of the ocean drilling program, scientific results, v. 116, p. 25-34. Ocean Drilling Program College Station TX.

Stow, D.A.V. and Tabrez, A.R., 1998, Hemipelagites: processes, facies and model. *in* Stoker, M.S., Evans, D., and Cramp, A., eds, Geological processes on continental margins: Sedimentation, mass-wasting and stability: Geological Society, London, Special Publication, v. 129, p. 317-337.

Talling, P.J., Masson, D.G., Sumner, E.J., and Malgesini, G., 2012, Subaqueous sediment density flows: depositional processes and deposits types: Sedimentology, v. 59, p. 1937-2003.
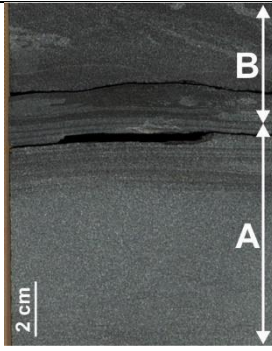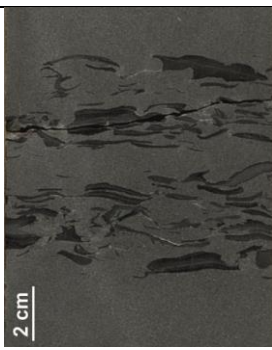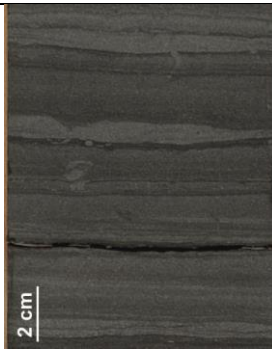
Talling, P.J., 2013, Hybrid submarine flows comprising turbidity current and cohesive debris flows: deposits, theoretical and experimental analyses, and generalized models: Geosphere, v. 9, p. 460-488.

Tankard, A., Welsink, H., Aukes, P., Newton, R., and Stettler, E., 2009, Tectonic evolution of the Cape and Karoo basins of South Africa: Marine and Petroleum Geology, v. 26, p. 1379-1412.

Trabucho-Alexandre, J., Dirkx, R., Veld, H., Klaver, G., and De Boer, P.L., 2012, Toarcian black shales in the Dutch Central Graben: record of energetic, variable depositional conditions during an oceanic anoxic event: Journal of Sedimentary Research, v. 82, p. 104-120.

Twichell, D.C., Schwab, W.C., Nelson, C.H., and Lee, H.J., 1992, Characteristics of a sandy depositional lobe on the outer Mississippi fan from SeaMARC IA sidescan sonar images: Geology, v. 20(8), p. 689-692.

Van der Werff, W., and Johnson, S., 2003, High resolution stratigraphic analysis of turbidite system, Tanqua Karoo Basin, South Africa: Marine and Petroleum Geology, v. 20, p. 45–69.

Veevers, J.J., Cole, D.I., and Cowan, E.J., 1994, Southern Africa: Karoo Basin and Cape Fold Belt. *in* Veevers, J.J., and Powell, C.M., eds., Permian-Triassic Pangean Basins and foldbelts along the Panthalassan margin of Gondwanaland, The Geological Society of America, Boulder, CO. Geological Society America, Memoir, v. 184, p. 223-279.

Viglietti, P.A., Rubidge, B.S., and Smith, R.M., 2017, New Late Permian tectonic model for South Africa's Karoo Basin: foreland tectonics and climate change before the end-Permian crisis: Scientific Reports, v. 7.

Viljoen, J.H.A., 1994, Sedimentology of the Collingham Formation, Karoo Supergroup: South African Journal of Geology, v. 97, p. 167-183.

Visser, J.N.J., and Praekelt, H.E., 1996, Subduction, mega-shear systems and Late Palaeozoic basin development in the African segment of Gondwana: Geologische Rundschau, v. 85(4), p. 632-646.

Visser, J.N.J., 1992, Deposition of the early to late Permian Whitehill Formation during a sea-level highstand in a juvenile foreland basin: South African Journal of Geology, v. 95 (5-6), p. 181-193.

Walker, R.G., 1978, Deep-water sandstone facies and ancient submarine fans – models for exploration and for stratigraphic traps: AAPG Bulletin, v. 62, p. 932-966.

Weaver, P.P.E., Rothwell, R.G., Ebbing, J., Gunn, D., and Hunter, P., 1992, Correlation, frequency of emplacement and source directions of megaturbidites on the Madeira Abyssal Plain: Marine Geology, v. 109(1-2), p. 1-20.

Wetzel, A., and Uchman, A., 2012, Hemipelagic and pelagic basin plains: Developments in Sedimentology, v. 64, P. 673-701. Elsevier

Wickens, H.D.V., 1994, Basin floor fan building turbidites of the southwestern Karoo Basin, Permian Ecca Group, South Africa [PhD Thesis]: University of Port Elizabeth, Port Elizabeth, South Africa, 233 p.

Wild, R., Flint, S.S., and Hodgson, D.M., 2009, Stratigraphic evolution of the upper slope and the shelf edge in the Karoo Basin, South Africa: Basin Research, v. 21, p. 502-527.

Wood, A., and Smith, A.J., 1959, The sedimentation and sedimentary history of the Aberystwyth Grits (Upper Llandoverian): The Quarterly Journal of the Geological Society of London, v. 114, p. 163-195.

Zachos, J., Pagani, M., Sloan, L., Thomas, E., and Billups, K., 2001, Trends, rhythms, and aberrations in global climate 65 Ma to present: Science, v. 292(5517), p. 686-693.

Table 1: Sandstone facies (Facies 5-10) of the Skoorsteenberg Formation, from current observations integrated with previous works.

Facies	Grain size	Bed Thickness Range	Description	Depositional Processes	Facies Association	Core Photograph
Structureless sandstone (F5)	Very fine to fine sandstone	0.4-4 m	Structureless; sharp, erosional or loaded base; common flute and tool marks; common dewatering.	Deposited by high-density turbidity currents (Lowe 1982; Kneller and Branney 1995). High aggradation rate (Arnott and Hand 1989; Leclair and Arnott 2005; Talling et al. 2012).	Channel axis, lobe axis, off-axis	
Structured sandstone (F6)	Very fine to fine sandstone	0.1-0.7 m	Planar, current-ripple, low-angle climbing-ripple or wavy laminations; normal grading; bed bases sharp or loaded; bed tops sharp and flat or undulating.	Deposited by low-density turbidity currents. Planar and current-ripple lamination produced by tractional reworking of bed tops by flows (Allen 1982; Southard 1991; Best and Bridge 1992). Climbing-ripple lamination associated with high aggradation rates (Allen 1973; Hunter 1977; Jobe et al. 2012). Wavy lamination associated with waning flows and high rates of suspension fallout (Jopling and Walker 1968; Allen 1973; Hunter 1977).	Lobe off-axis	

Hybrid bed (F7)	Very fine to fine sandstone	0.05-1.5 m	Lower subdivision (A) with well sorted and "clean" sandstone; upper subdivision (B) can be: (1) mudstone-clast rich with clean matrix; (2) argillaceous, poorly sorted sandstone with swirly and patchy fabric comprising mudstone chips and wood fragments.	Deposited from strongly stratified transitional flows (Baas et al. 2011; Kane and Pontén 2012; Talling et al. 2013; Kane et al. 2017) or from co-genetic turbidity currents (lower division) and cohesive debris flows (upper division) (Haughton et al. 2003; Haughton 2009; Hodgson 2009).	Lobe axis, off-axis, fringe	
Debrite (F8)	Very fine to fine sandstone	0.2-3 m	Poorly sorted; mud-rich; outsize grains; mudstone chips; wood fragments.	Deposited by *en masse* freezing of cohesive debris flows (Iverson 1997; Talling et al. 2012).	Channel axis, lobe axis, off-axis, fringe	
Very thin- to thin-bedded sandstone (F9)	Coarse mudstone to very fine mudstone	0.05-0.3 m	Planar, wavy and current-ripple lamination; normal grading; sharp and erosional bed bases; undulating tops due to preservation of ripple crests.	Deposited by low-density turbidity currents. Ripple lamination form beneath dilute turbulent flows via reworking of the bed under moderate aggradation rates (Allen 1971; Allen 1982; Southard 1991).	Fringe, distal fringe	

Ash-rich sandstone (F10)	Very fine to fine sandstone	0.02-0.3 m	Planar and current-ripple lamination; normal grading or ungraded; sharp or erosional bases; brownish to greenish color.	Normally-graded bed deposited by low-density turbidity currents. Ungraded beds deposited by vertical suspension fallout.	Lobe distal fringe, basin plain	
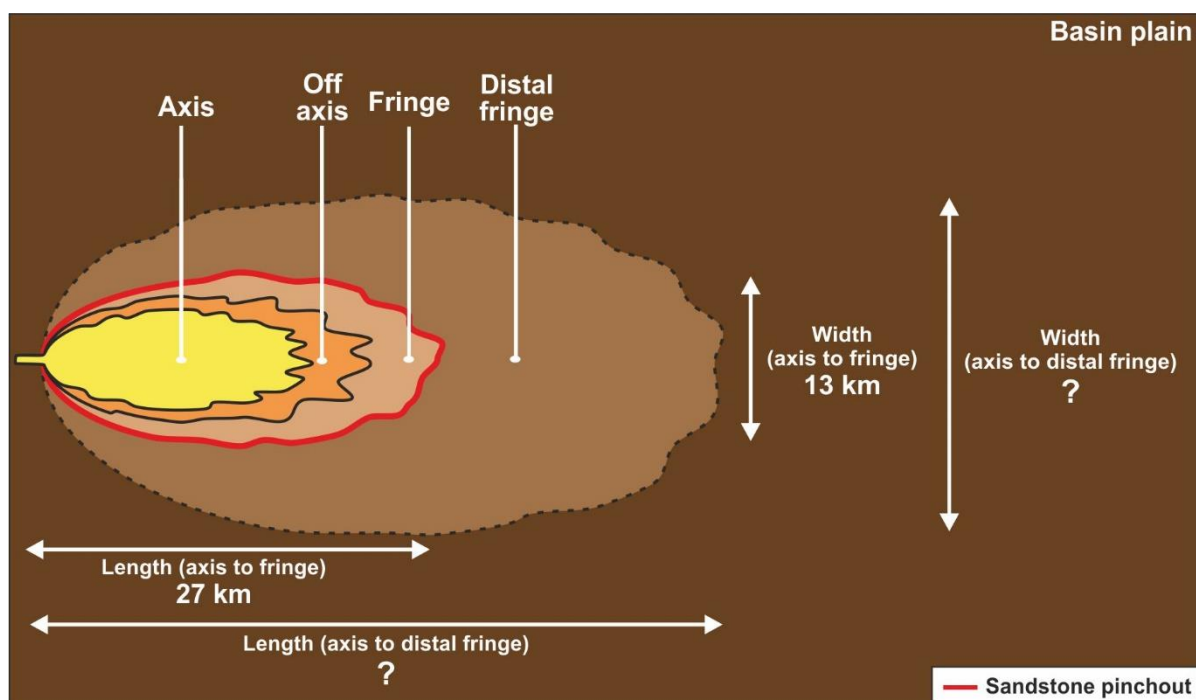
Figure 1: Simplified plan-form view of lobe sub-environments. Average lobe dimensions are from Fan 3 of the Skoorsteenberg Formation (Karoo Basin, Tanqua depocenter; Prélat et al. 2009). Redrawn from Prélat et al. (2009).
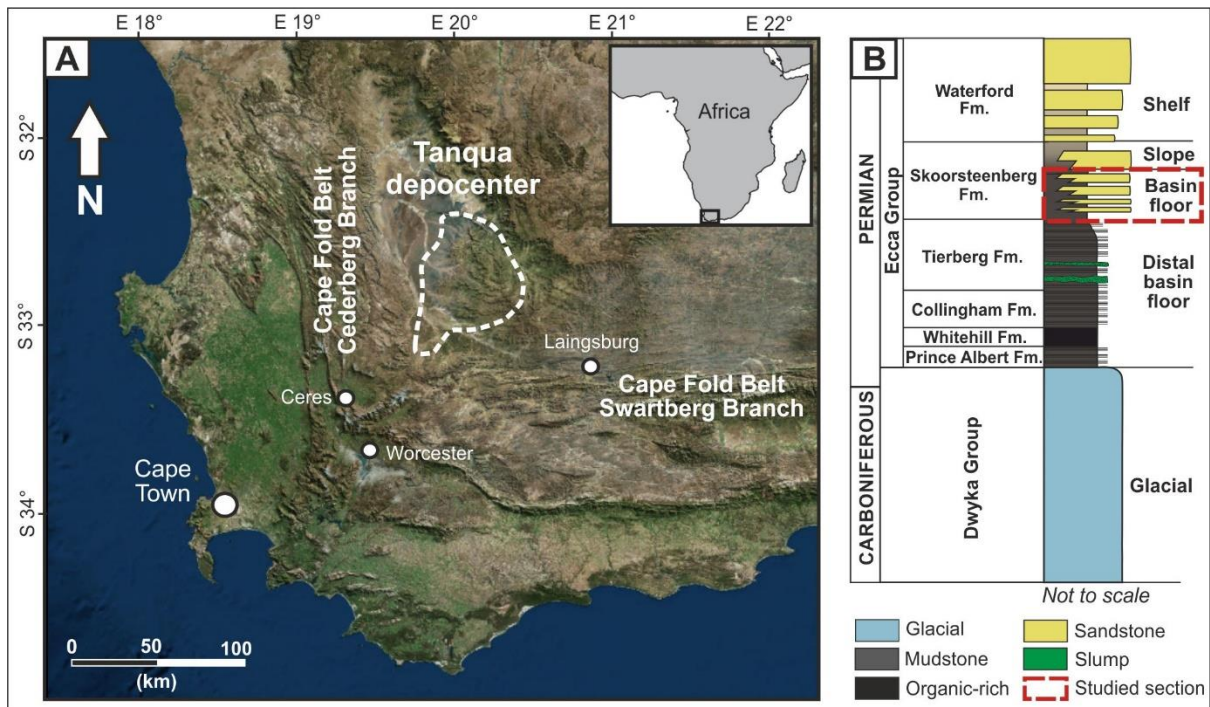
Figure 2: A) Satellite view of southwest South Africa with location of study area (Tanqua depocenter, Karoo Basin) indicated by the white square. **B)** Schematic stratigraphic log of Karoo Supergroup in the Tanqua depocenter. Stratigraphy presented in this study indicated by the red dotted square. Modified after Wickens (1994).
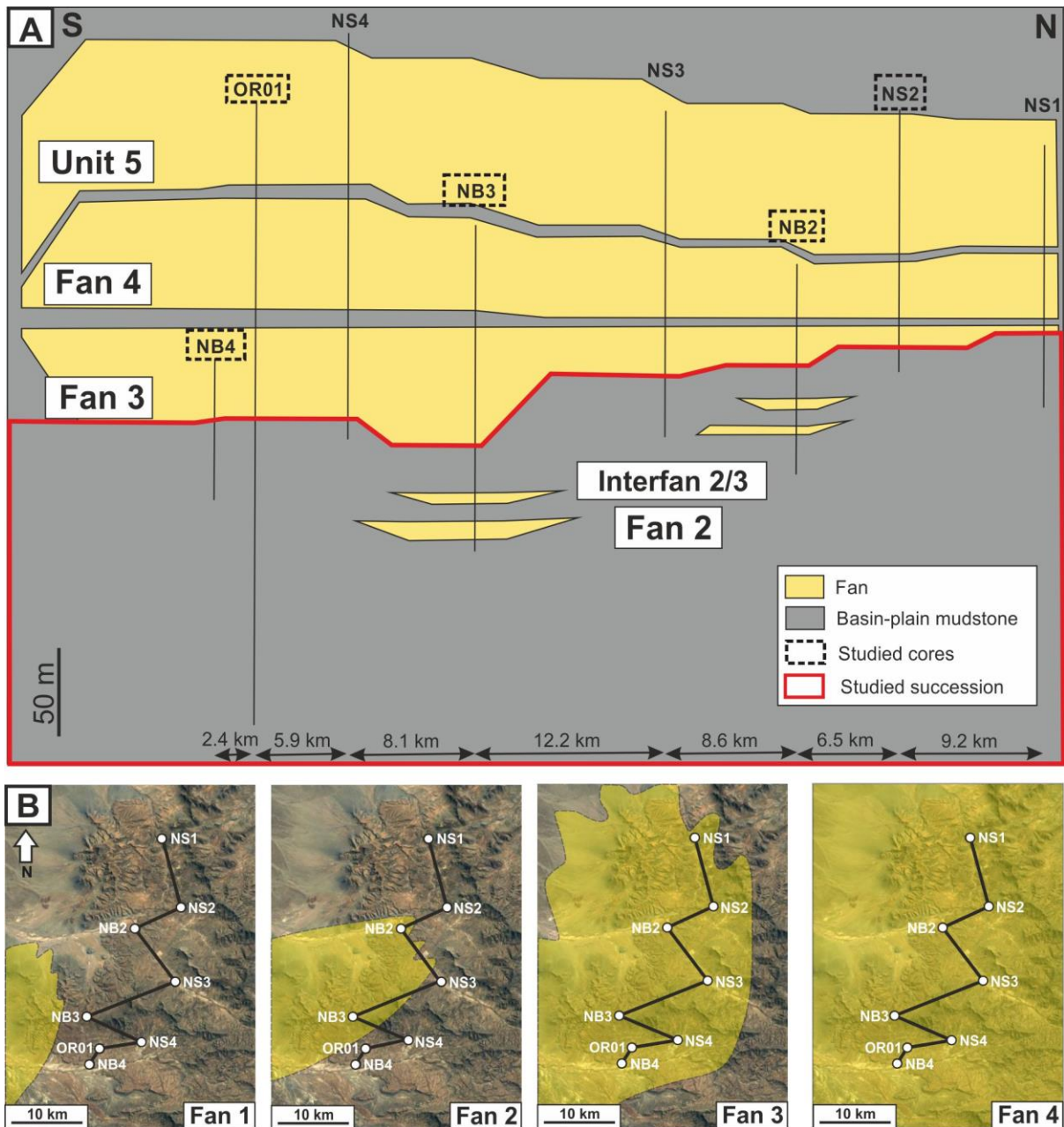
Figure 3: A) Simplified correlation panel of Fan 2-4 and Unit 5. Fan 1 is not encountered in the subsurface. The apparent lenses shape of Fan 2 and Interfan 2/3 is due to the change of direction of correlation. Modified from Hodgson et al. (2006). **B)** Satellite view of study area (Tanqua depocenter) with interpreted paleogeographical extent of Fans 1-4. Interpretation based on outcrops mapping integrated with core data. Modified from Hodgson et al. (2006) and Hansen et al. (2019).

	Core	Thin Section

Facies 1 — Normally graded very thin-bedded mudstone

A — Fig. 4B — 1 cm

B — 5 mm

Mottled beds
Normal grading
Mottled beds
Flame structure
Planar-parallel laminations
(cm) fm cm

Facies 2 — Discontinuous very-thin bedded mudstone

C — Fig. 4D — 1 cm

D — 5 mm — erosional base

Erosional base
Discontinuous bed contact
Discontinuous laminae
Mottled normally-graded bed
(cm) fm cm

Facies 3 — Very thin- to medium-bedded structureless mudstone

E — Fig. 4F — 1 cm

F — 5 mm

Pyrite nodule
Erosional base
Mottled texture
Discontinuous laminae
(cm) fm cm

Facies 4 — Mottled mudstone

G — Fig. 4H — 1 cm

H — 5 mm

Pyrite nodules
Discontinuous laminae
Pyrite nodules
Discontinuous laminae
(cm) fm cm

Figure 4: Illustration of the four mudstone facies identified in the Skoorsteenberg Formation from OR01 core. White dotted squares in core views indicate locations of thin-section scans. **A)** Facies 1 (Normally graded very thin-bedded mudstone). Dry core photograph (260.11 m). **B)** Thin-section scan with microstratigraphic log section. Stacked normally-graded mudstone beds. Sharp erosional base. Planar-parallel laminations only observed at the base of the thickest beds. Bioturbation weak to sparse (BI: 1-2). Note the flame structures at the base of the bed at 1.1 cm. **C)** Facies 2 (Discontinuous very thin-bedded mudstone). Dry core photograph (216.80 m). Beds usually laterally discontinuous and hard to spot at core scale. **D)** Thin-section scan with microstratigraphic log section. Bioturbation is strong (BI: 4). Some bed bases highlighted by white arrows. Rare preserved normal grading. Rare planar-parallel laminations. **E)** Facies 3 (Very thin- to medium-bedded structureless mudstone). Dry core photograph (244.41 m). **F)** Thin-section scan with microstratigraphic log section. Mottled texture with bed contact and discontinuous laminae. The lighter color above the erosional base is due to a lower clay content. **G)** Facies 4 (Mottled mudstone). Dry core photograph (147.80 m). Homogeneous and structureless texture at core scale. **H)** Thin-section scan with microstratigraphic log section. Note the discontinuous bed contact and the very small burrows. Common pyrite nodules.
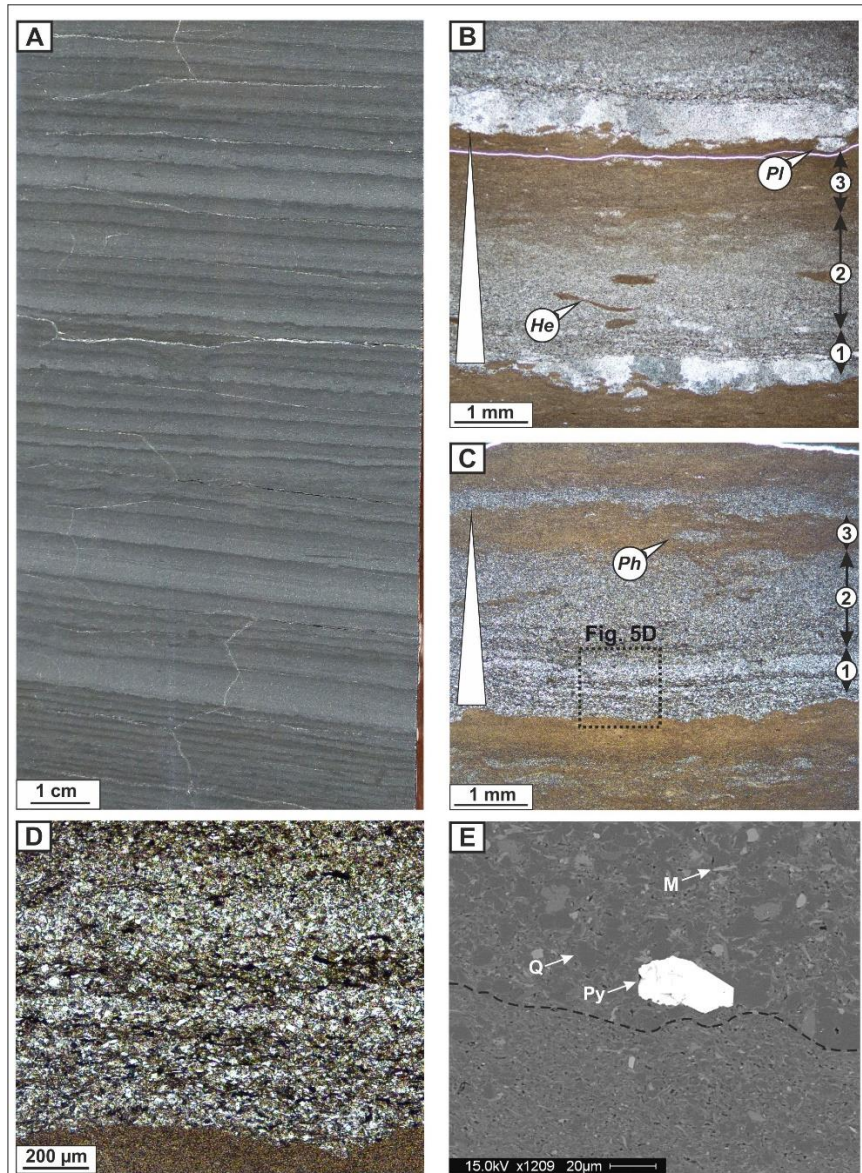
Figure 5: Facies 1 (Normally graded very thin-bedded mudstone) examples of key features from OR01 core. **A)** Wet core photograph (265.55 m). Stacked erosional normally graded beds. Note the upward decrease of bed dip angle and the weak to sparse bioturbation (BI: 1-2). **B)** Optical microscope photograph (260.11 m). Erosional normally graded bed with tripartite microstratigraphy. Lower subdivision (1) consists of planar parallel laminated coarse mudstone. Middle subdivision (2) consists of structureless normally graded coarse mudstone. Upper subdivision (3) consists of mottled fine mudstone. Gradual transition from middle to upper subdivision. Bed base characterized by calcium carbonate cementation. Increasing upward bioturbation. *He = Helminthopsis, Pl = Planolites.* **C)** Optical microscope photograph (145.03 m). Tripartite erosional normally graded beds. Sharp transition from the middle to upper subdivision. *Ph = Phycosiphon.* **D)** Optical microscope photograph (145.03 m). Zoom on the lower subdivision. Alternation of clay-rich (dark color) and quartz-rich (light color) laminae. **E)** BSE SEM image (260.11 m). Erosional bed base characterized by transition from fine to coarse mudstone. Q= Quartz, M = Mica, Py = Pyrite.
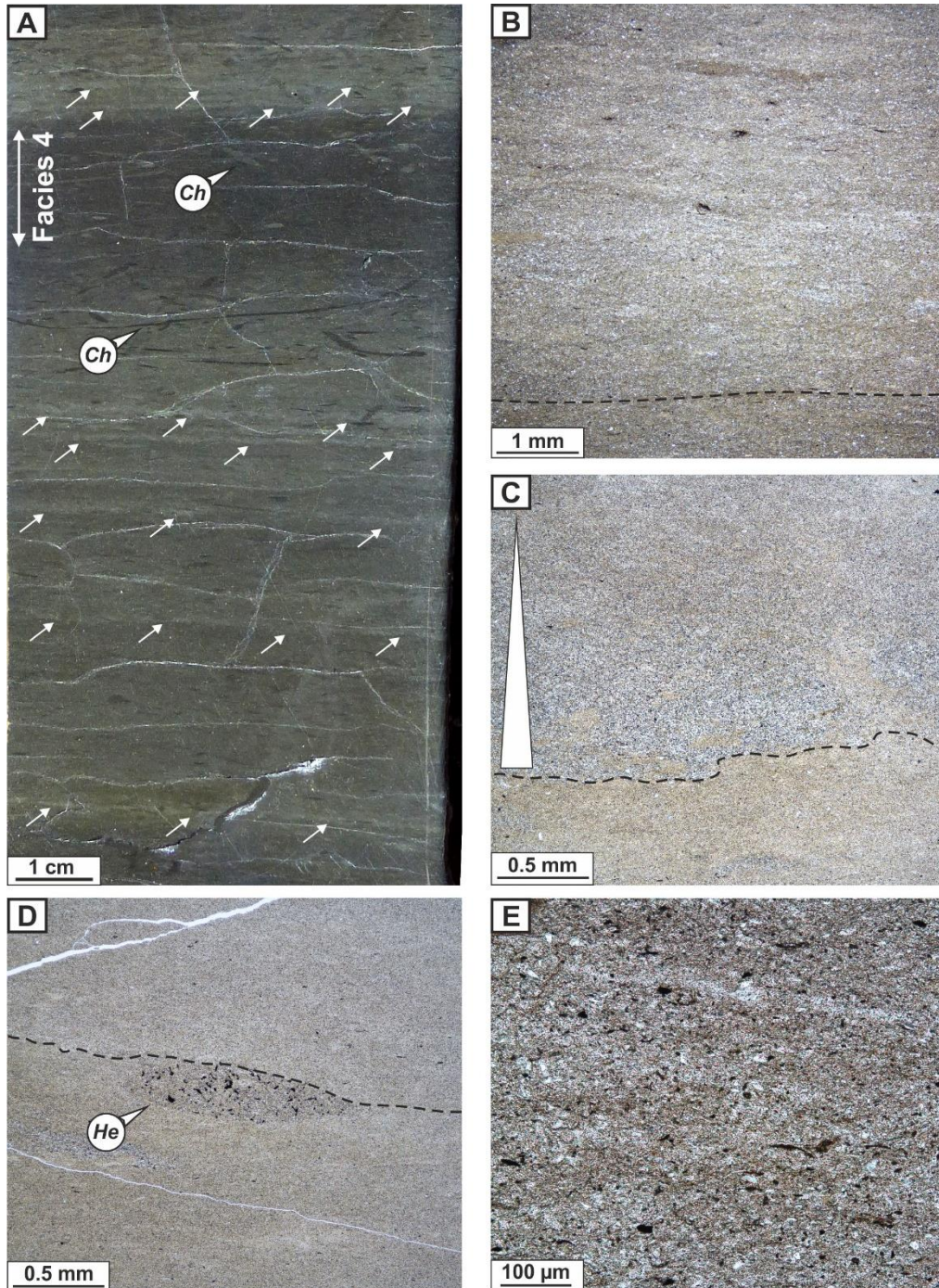
Figure 6: Facies 2 (Discontinuous very thin-bedded mudstone) examples of key features from OR01 core. **A)** Wet core photograph (218.13 m). Laterally discontinuous very thin beds highlighted by white arrows. *Ch = Chondrites*. **B)** Optical microscope photograph (328.76 m). Mottled very thin bed. Bed base is hard to recognize due to strong bioturbation. **C)** Optical microscope photograph (291.74 m). Erosional normally graded beds. **D)** Optical microscope photograph (291.74 m). Erosional normally graded beds. Bed base is hard to recognize due to strong bioturbation. *Helminthopsis (He)* burrow preferentially filled with pyrite. **E)** Optical microscope photograph (328.76 m). Texture consists mostly of clay, quartz, feldspar and organic fragment, similar to Facies 1.

47
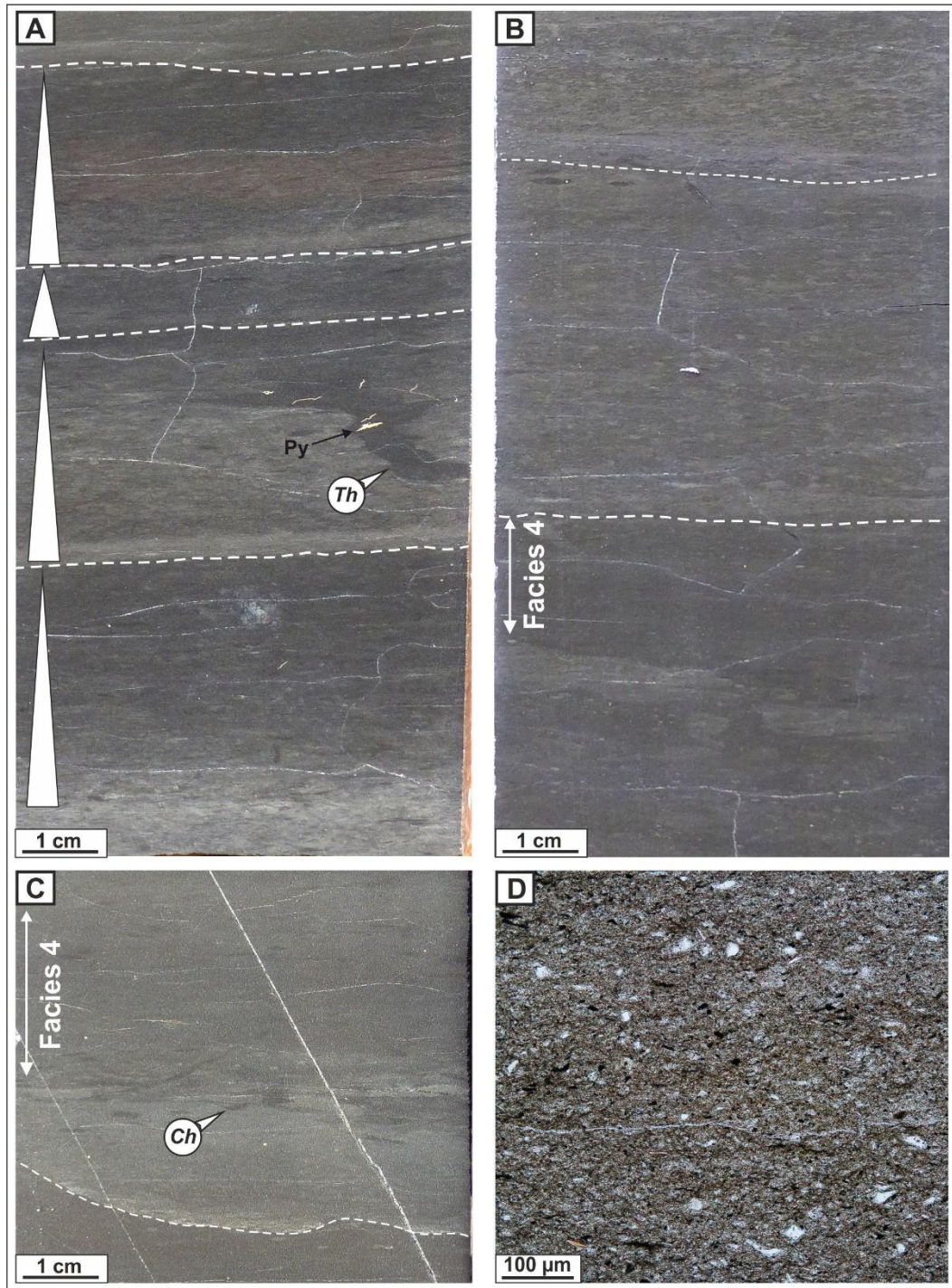
Figure 7: Facies 3 (Very thin- to medium-bedded structureless mudstone) examples of key features from OR01 core. **A)** Wet core photograph (308.44 m). Stacked normally graded structureless very thin- to medium-bedded mudstone. Bioturbation is pervasive across the beds. Note the *Thalassinoides* burrow (*Th*) preferentially filled with pyrite (Py). **B)** Wet core photograph (335.30 m). Stacked normally graded thin-bedded mudstone overlying Facies 4. **C)** Wet core photograph (385.50 m). Scoured bed base overlain by slightly normally graded thin-bedded mudstone. Note the *Chondrites* burrows (*Ch*) on top of the bed **D)** Optical microscope photograph (374.25 m). Texture consists mostly of clay with rare quartz, feldspar and organic fragment.
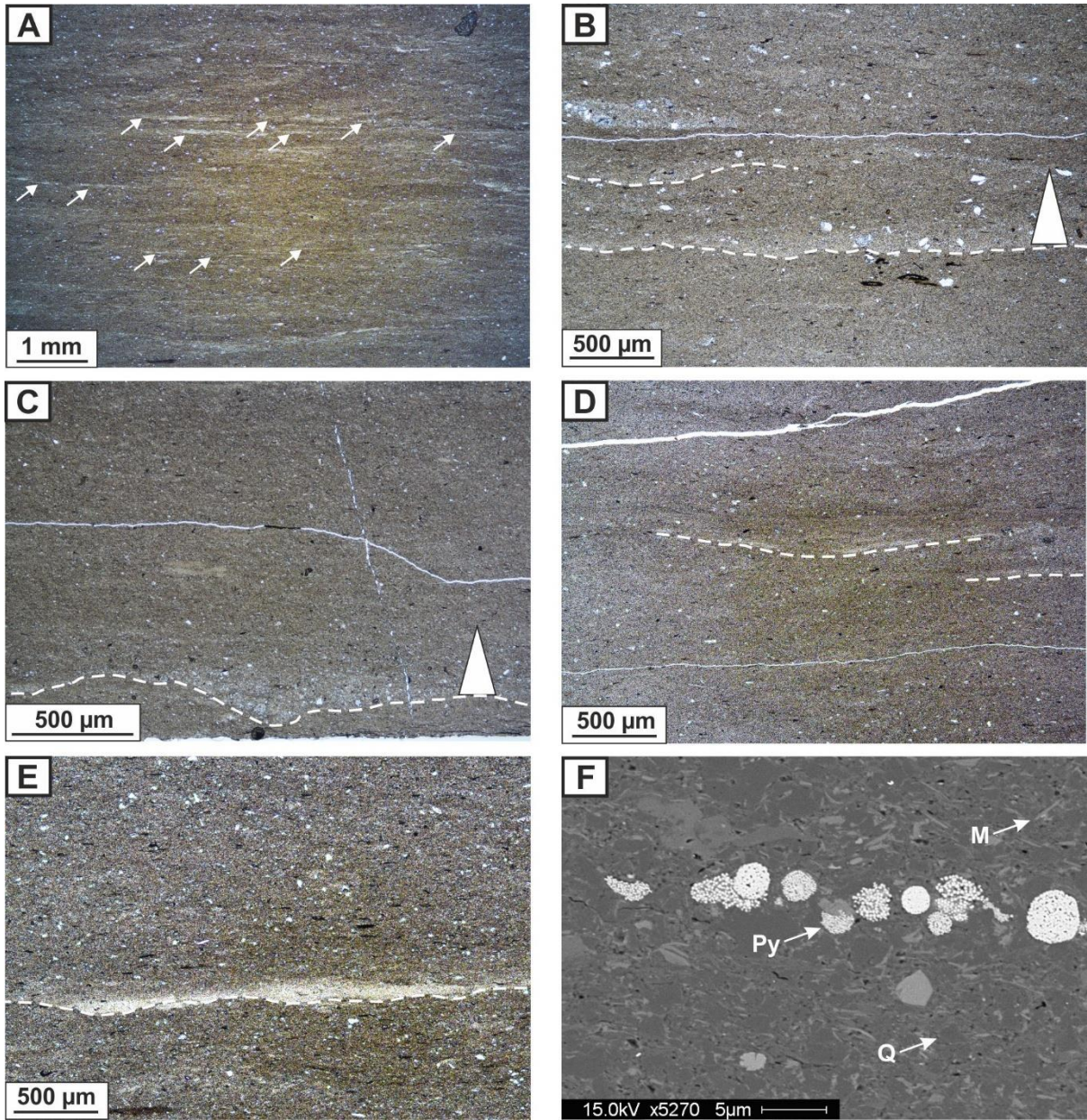
Figure 8: Facies 4 (Mottled mudstone) examples of key features from optical microscope photograph from OR01 core. **A)** Discontinuous laminae highlighted by white arrows (147.80 m). **B)** Erosional weakly normally graded bed (274.04 m). **C)** Scour overlain by normally graded coarse mudstone (219.80 m). **D)** Laterally discontinuous erosional bed base (348.20 m). **E)** Erosional bed base (237.55 m). **F)** BSE SEM image showing an example of texture in Facies 4 (366 m). Q = Quartz, M = Mica, Py = Pyrite.
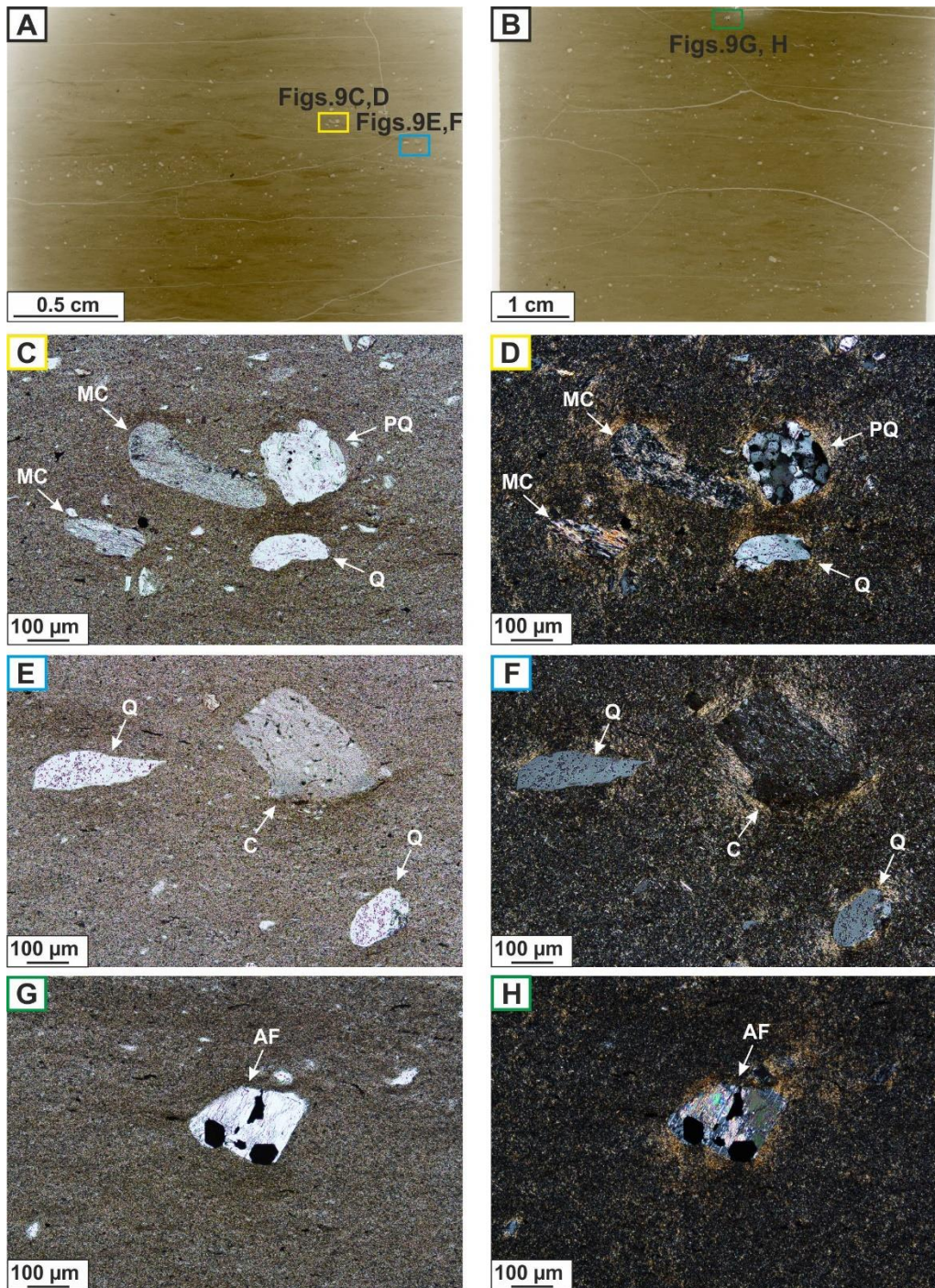
Figure 9: Floating outsize grains in Facies 4 from OR01 core. **A)** Thin-section scan (106.76 m). Localizations of Figures 9C, 9D, 9E and 9F shown by colored squares. **B)** Thin-section scan (107.11 m). Localizations of Figures 9G and 9H shown by colored squares. **C)** Optical microscope photograph (plane-polarized light). **D)** Optical microscope photograph (cross-polarized light). **E)** Optical microscope photograph (plane-polarized light). **F)** Optical microscope photograph (cross-polarized light). **G)** Optical microscope photograph (plane-polarized light). **H)** Optical microscope photograph (cross-polarized light). C = Chert, PQ = Polycrystalline quartz, Q = Quartz, MC = Metamorphic clast, AF = Altered feldspar.
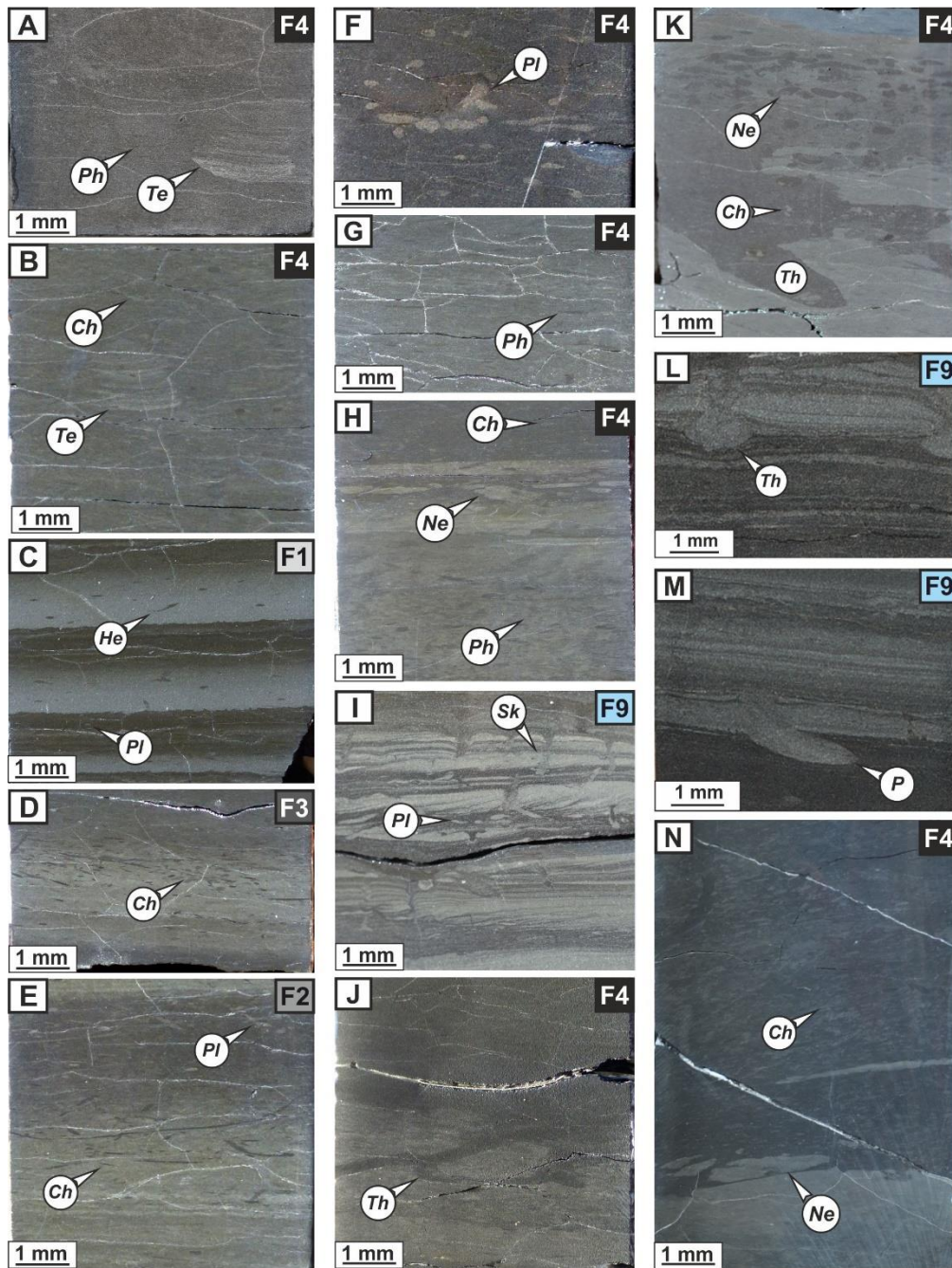
Figure 10: Core photographs of the range of ichnotaxa described in the Skoorsteenberg Formation from OR01 core. **A)** *Phycosiphon* and *Teichichnus* in Facies 4 (394 m). **B)** *Chondrites* and *Teichichnus* in Facies 4 (401.73 m). **C)** *Helminthopsis* and *Planolites* in Facies 1 (258 m). **D)** *Chondrites* in Facies 3 (286.92 m). **E)** *Chondrites and Planolites* in Facies 2 (218.13 m). **F)** *Planolites* in Facies 4 (250.80 m). Burrows are cemented by calcium carbonate. **G)** *Phycosiphon* in Facies 4 (270.30 m). **H)** *Chondrites, Nereites* and *Phycosyphon* in Facies 3 (378.30 m). **I)** *Planolites* and *Skolithos* in Facies 9 (115.90 m). **J)** *Thalassinoides* in Facies 4 (324.30 m). **K)** *Chondrites, Nereites* and *Thalassinoides* in Facies 4 (373.31 m). **L)** *Thalassinoides* in Facies 9 (149.05 m). **M)** *Palaeophycus* in Facies 9 (149.85 m). **N)** *Chondrites* and *Nereites* in Facies 4 (384 m).
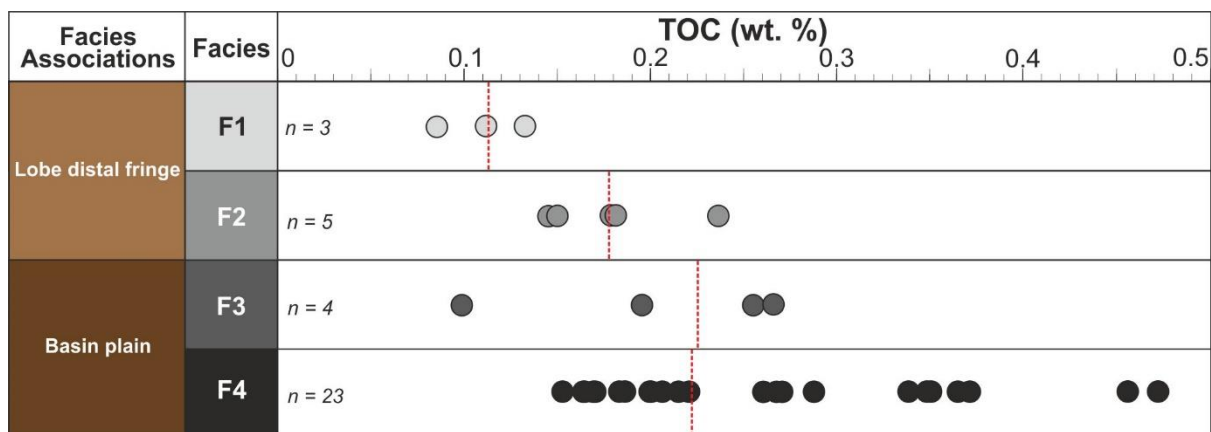
Figure 11: Total organic carbon (TOC) measurements, organized by facies and facies associations. Samples are from cores NB4, NB3 and NS2 cores. The dataset shows an increase of TOC from proximal to distal basin-floor environments.
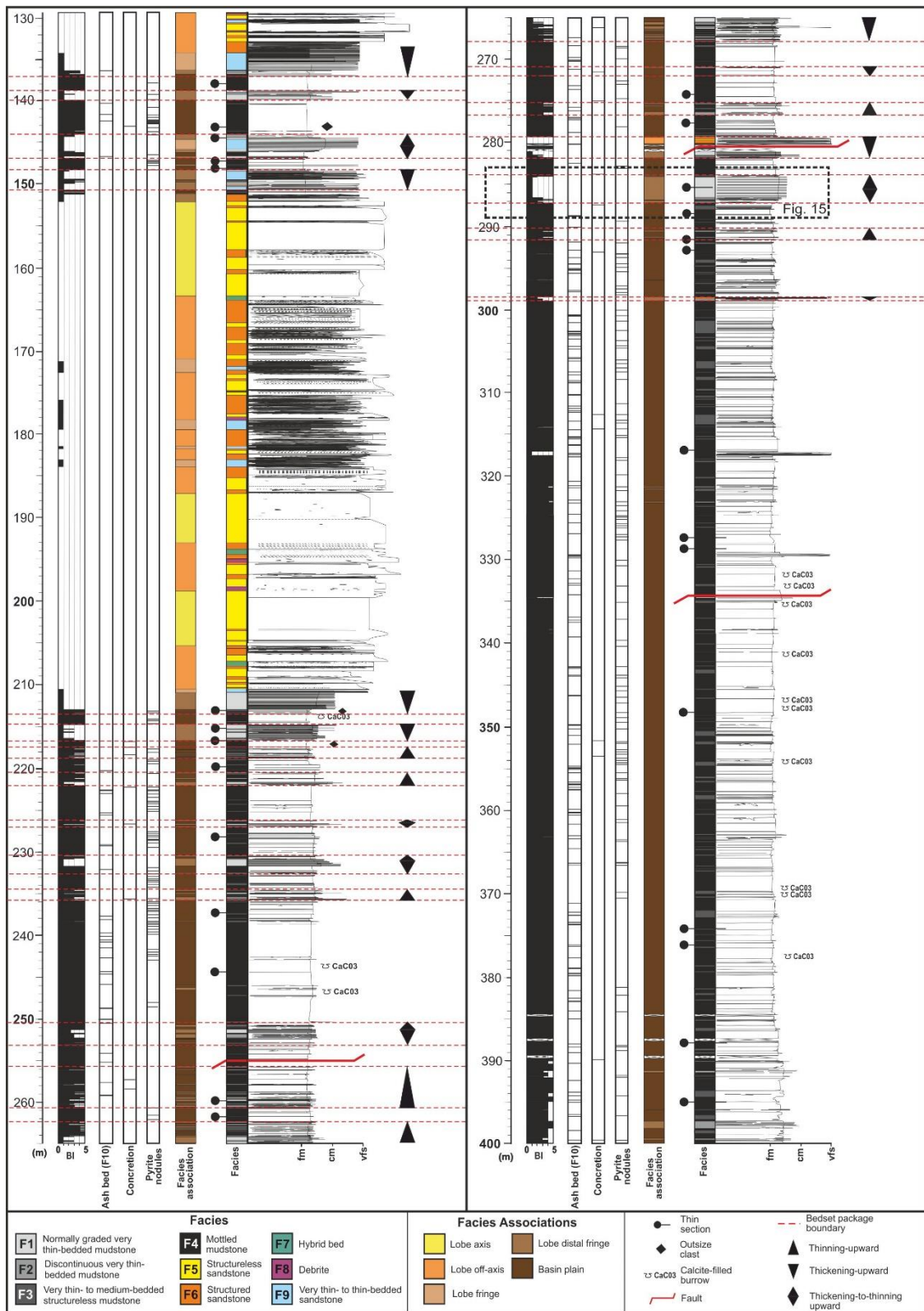
Figure 12: Summarized sedimentary log of OR01 core (from 400 m up to 130 m), including facies, facies associations, bioturbation intensity, macroscopic pyrite nodules and ash-rich sandstone beds (Facies 10). Bioturbation intensity scale from Droser and Bottjer (1986). fm = fine mudstone, cm = coarse mudstone, vfs = very fine sandstone.
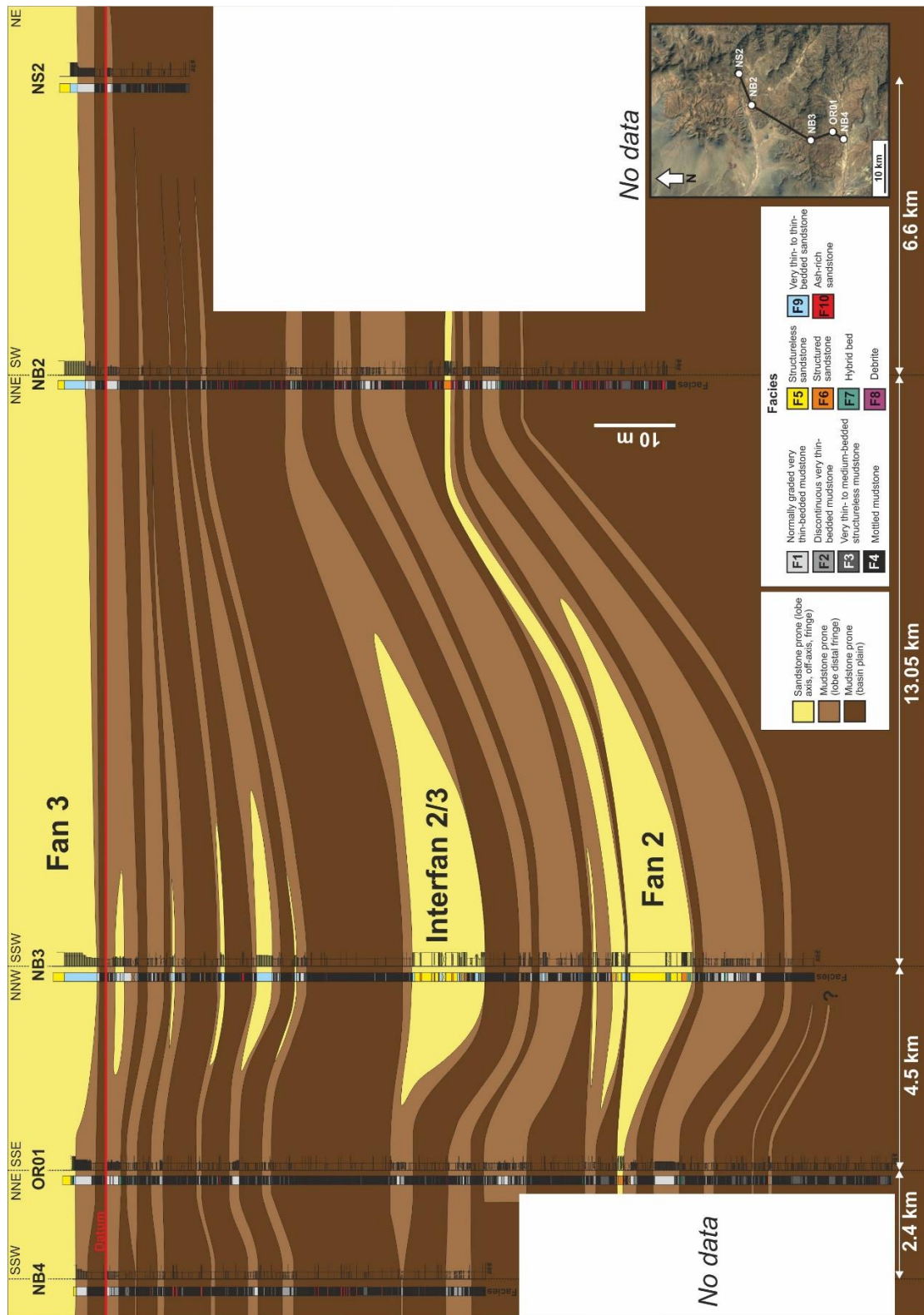
Figure 13: Correlation panel between the different cores (NB4, OR01, NB3, NB2, NS2). The datum for correlation is the base of the laterally continuous unit of basin plain mudstone dominated by Facies 3 and Facies 4 directly underlying Fan 3 (red line). Correlation of bedset packages dominated by very thin beds of Facies 1 and Facies 2 interpreted as lobes, separated by units dominated by basin plain deposits of Facies 3 and Facies 4.
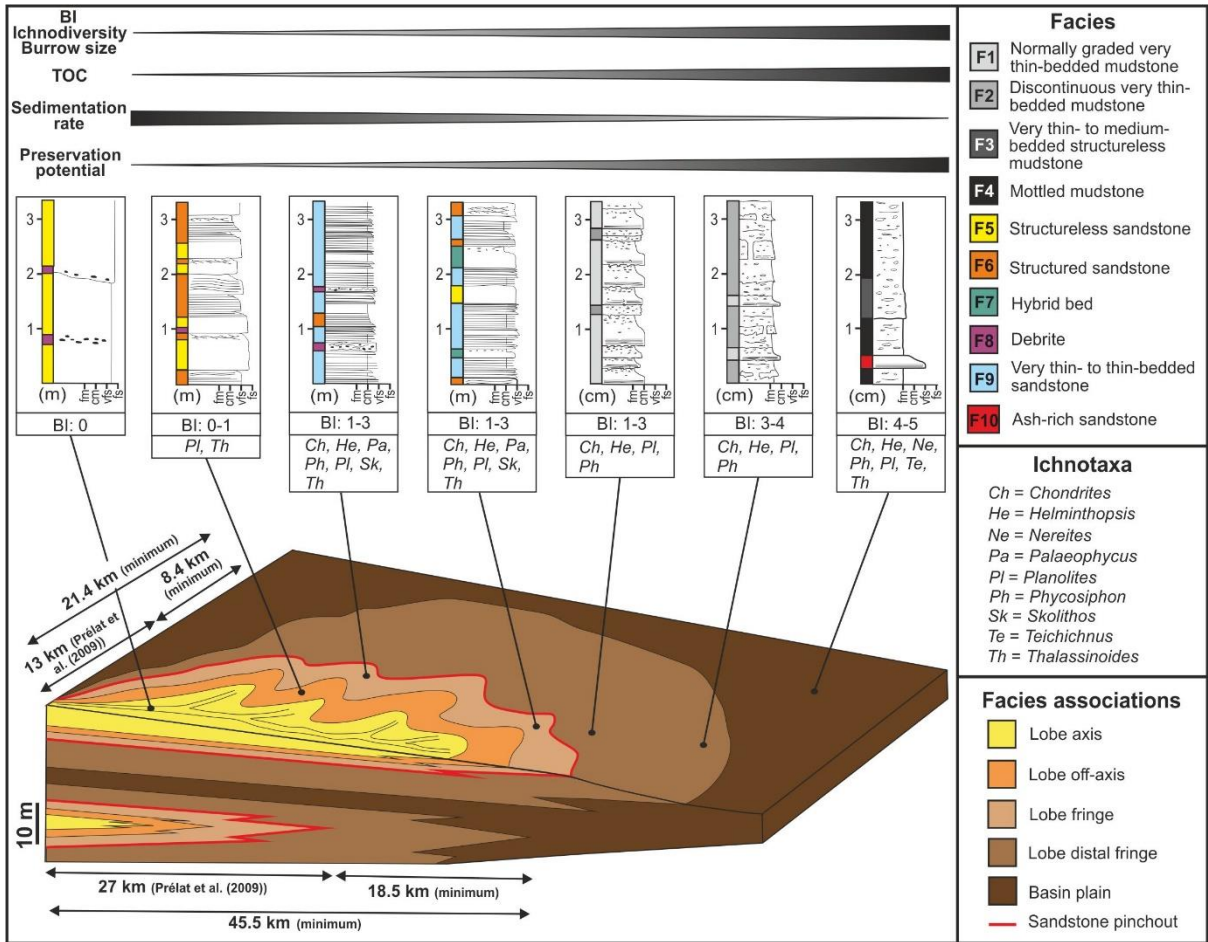
Figure 14: Depositional model of lobe sub-environments based on the description and interpretation of the lower part of the Skoorsteenberg Formation. Examples logs for each sub-environment are shown, along with ichnotaxa and bioturbation intensity (BI).
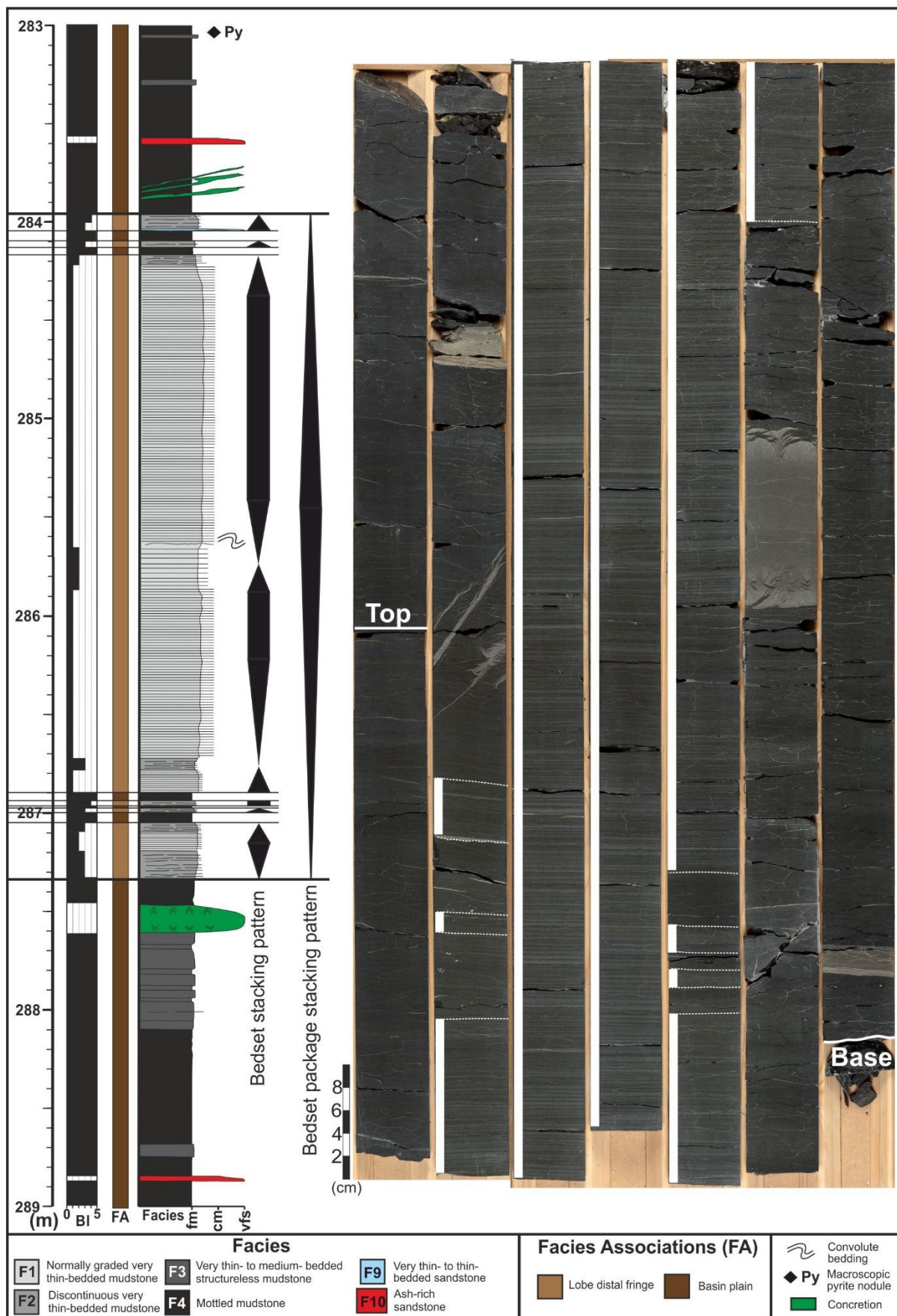
Figure 15: Example of stacking patterns within a mudstone-prone bedset package, interpreted as lobe (from 289 m to 283 m; OR01). See stratigraphic position in Figure 12.
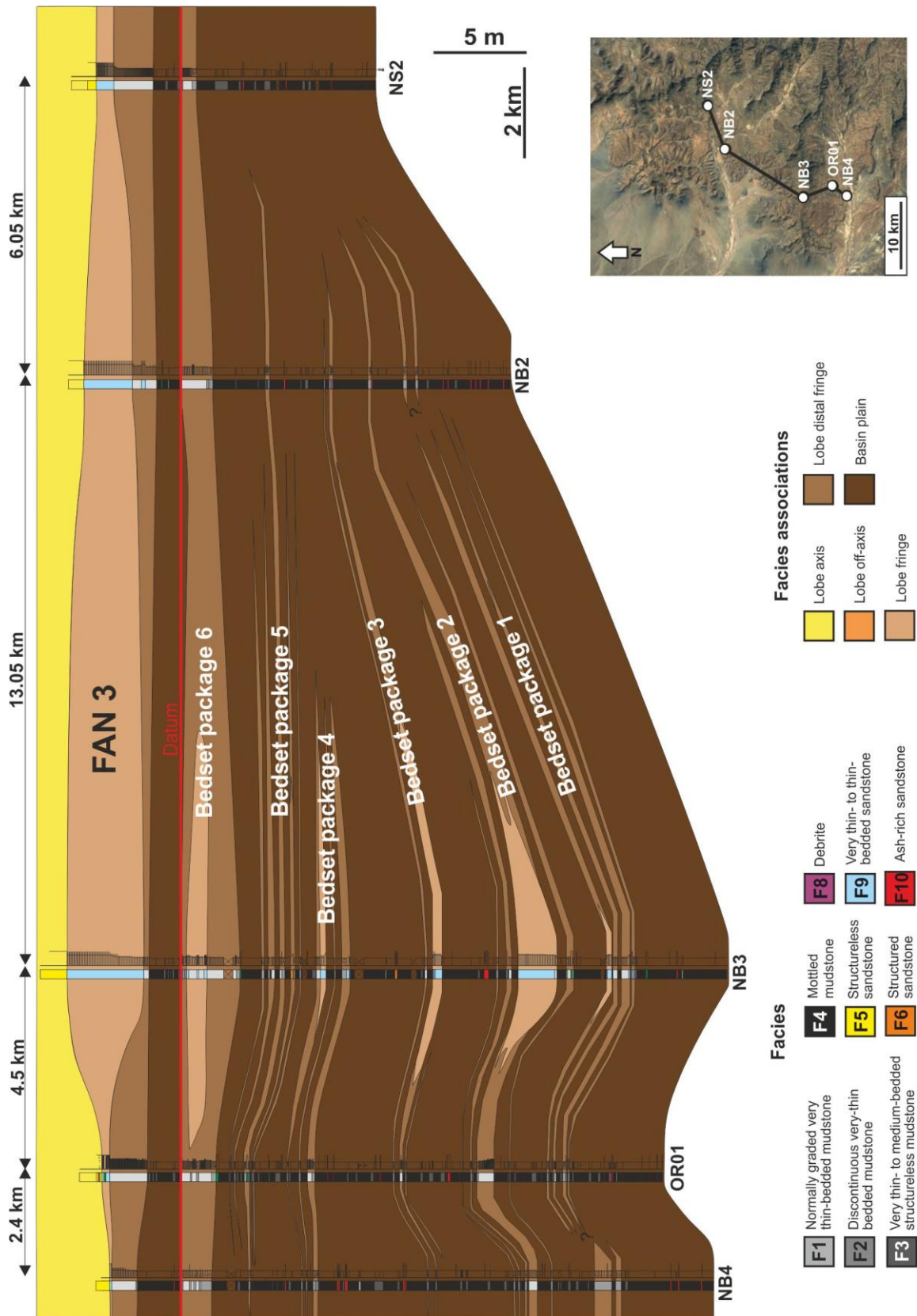
Figure 16: Correlation panel of the mudstone-prone succession below Fan 3. Facies associations have been correlated. Six bedset packages have been characterized, associated with thinning and finning away from core NB3.
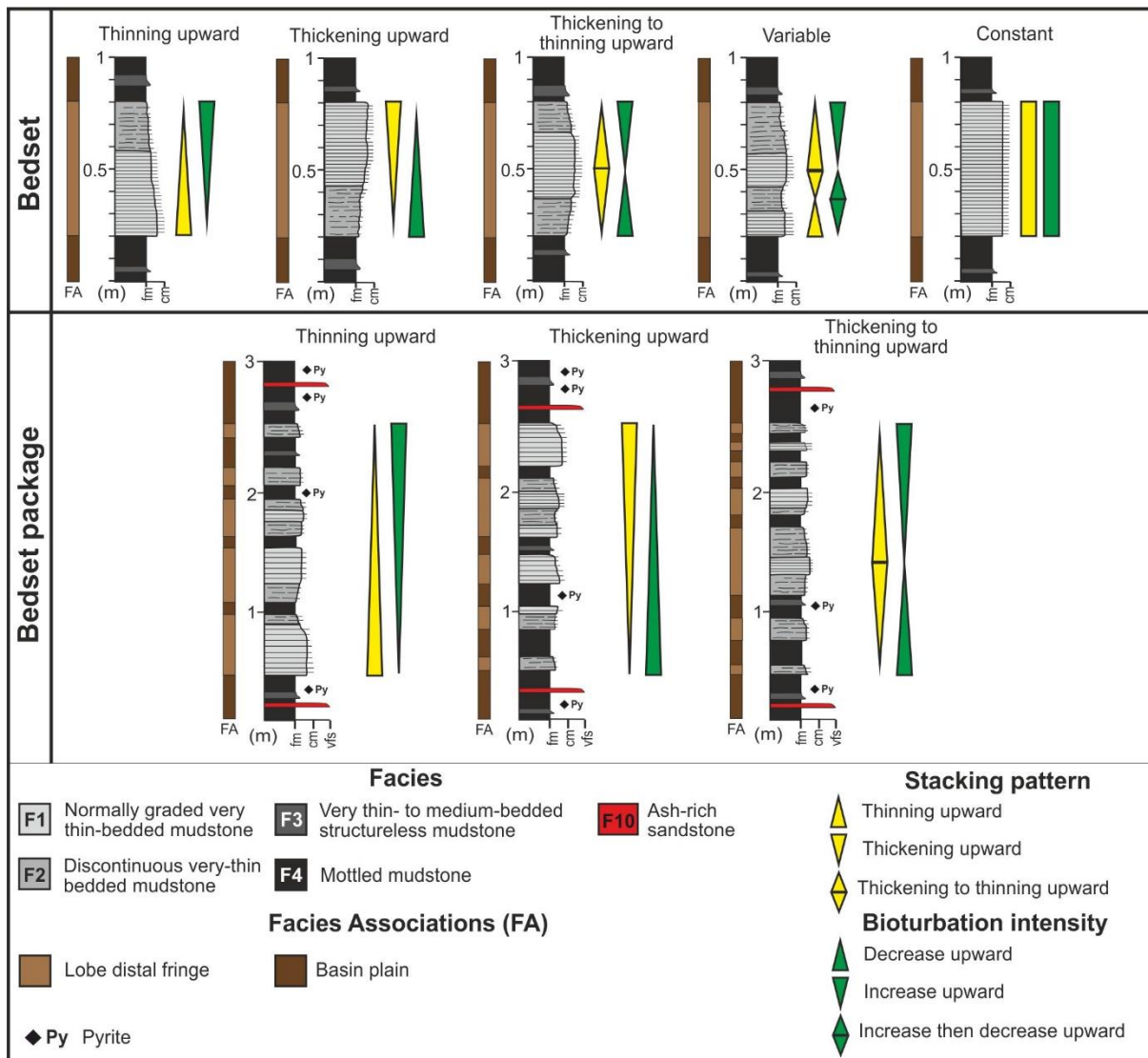
57

Figure 17: Schematic of idealized stacking pattern of bedsets and bedset packages in distal basin-floor fan environments. Bioturbation intensity is also indicated. Stacking pattern of mudstone-prone lobe distal fringe deposits is as variable as for more proximal sandstone-prone axis to fringe deposits. See Figure 12 and Figure 13 for example of stacking pattern within the succession.